

**Hygrothermal Performance Evaluation of Multi-functional Panels for Building Envelope in  
Various Climate Conditions**

by

Lana Secchi

A thesis submitted in partial fulfillment of the requirements for the degree of

Master of Science

in

Civil (Cross-Disciplinary)

Department of Civil and Environmental Engineering

University of Alberta

© Lana Secchi, 2020

## **ABSTRACT**

There is an increasing concern worldwide to discover ways to mitigate greenhouse gas emissions. Researchers are working in various industry sectors to discover environmentally-friendly solutions to produce goods and services. In the building sector, research focuses on the use of energy-efficient solutions for building design, construction, and operation. The research presented in this thesis investigates and evaluates the long-term hygrothermal performance of multi-functional panels (MFPs) in various wall assembly configurations to improve energy efficiency for residential buildings under varying climatic conditions. The MFPs are used as an additional layer attached to the exterior side of conventional wood-frame wall assemblies. The MFPs under investigation combine two layers of wood sheathing with other elements, such as wood fibre and Extruded Polystyrene (XPS) insulation, as additional external layers to conventional light wood-frame wall assemblies in order to improve the overall energy efficiency of conventional wall assemblies. Field monitoring data was collected for two years, was analyzed, and comparisons between the two MFPs and a conventional wall assembly were made. For a complete analysis, the evaluation was conducted using real-life scenarios in test huts situated in two different climates in Canada: Vancouver, British Columbia, with a coastal humid climate; and Edmonton, Alberta, with an extremely cold climate in winter. This study will provide a field hygrothermal investigation for the application of wood fibre insulation—an environmentally-friendly and recyclable material—for the North American housing market.

## **Preface**

This thesis is the original work by Lana Secchi under the supervision of Dr. Mustafa Gul. The related topics to this research and paper writing were finished by Lana Secchi with guidance from Dr. Mustafa Gul. One conference paper related to this project was published and one journal paper is under revision with Lana Secchi as a second author as listed below.

## **List of Proceedings**

Secchi, L., Awad, H., Salim, K., Gul, M., Knudson, R. “Hygrothermal field testing of multi-functional wood fibre panels for residential buildings” 1<sup>st</sup> International Conference on New Horizons in Green Civil Engineering (NHICE-01), Victoria, BC, Canada, April 25-27, 2018.

Awad, H., Secchi, L., Gul, M., Ge, H., Knudson, R., Al-Hussein, M. “Thermal resistance of Multi-functional panels in cold-climate regions”. Accepted (2020) at Journal of Building Engineering.

## **Acknowledgements**

First, I would like to thank my supervisor, Dr. Mustafa Gül, for his guidance and support throughout this research. Also, I would like to express my deepest gratitude to Dr. Hadia Awad, a friend and partner in this research project, for her valuable contributions. I am also so grateful to the committee members, Dr. Mohamed Al-Hussein, Dr. Yuxiang Chen, and Dr. Michael Hendry, for their insightful comments and challenging questions.

In addition, I am grateful for the support from the administrative and research staff of Dr. Al-Hussein's research group at the University of Alberta, especially my friend Claire Black. Great thanks to my colleagues, Samer, Regina, Beda, Chelsea, Osama, and Marko, and a special thanks to my friends Mahmud and Harish for bringing me joy during tough times.

I would like to extend my gratitude to all my family and friends for their continuous love and encouragement. I am especially grateful to my mom and dad for always inspiring me to do my best, and to my sisters and nieces for their endless love. I would like to dedicate this work to my husband, Vini, who has given me strength, love, and encouragement to never give up, and to my lovely kids, Pedro and Bella, for making me a better person and lighting up my days.

## Table of Content

ABSTRACT.....	ii
Preface.....	iii
List of Proceedings .....	iii
Acknowledgements.....	iv
List of Tables .....	vii
List of Figures.....	viii
Chapter 1 Introduction .....	1
1.1 Research Objectives.....	3
1.2 Organization of Thesis.....	4
Chapter 2 Literature Review.....	5
2.1 Materials for Building Envelope.....	5
Environmentally friendly materials .....	5
Multi-functional panels (MFPs).....	9
2.2 Review on Hygrothermal Performance Evaluation .....	10
Chapter 3 Experimental Setup and Implementation .....	18
3.1 Multi-functional Panels (MFPs) .....	18
3.2 Test Huts .....	21
3.3 Sensor Types and Layout.....	23
3.4 Indoor Ambient Conditions .....	27
3.5 Location and Climate Conditions .....	29
Chapter 4 Hygrothermal Performance Analysis.....	34
4.1 Calculation of the Thermal Resistance from the Field Data.....	34
4.2 Indoor Temperature Distribution on Tested MFPs.....	43
4.3 Impact of Thermal Bridge and Thermal Mass Performance .....	49
4.4 Moisture Content Levels in the MFPs .....	53
4.5 Vapour Control in the Insulation Panels.....	57
4.6 Discussion of Hygrothermal Performance.....	61
Chapter 5 Conclusion.....	75
5.1 General Conclusion.....	75
5.2 Research Contributions.....	78
5.3 Research Limitations .....	79

5.4 Future Research .....	79
References .....	81

## List of Tables

Table 1: Thermal conductivity of binderless coconut husk insulation board (BCI) and binderless bagasse insulation board (BBI) compared with other insulation materials. ....	7
Table 2: Materials properties of samples. ....	8
Table 3: Sensor type and quantity used in experimental setup. ....	24
Table 4: Edmonton weather statistics. ....	31
Table 5: Vancouver weather statistics. ....	33
Table 6: RSI calculations–part 1: sample time series raw data as temperature and heat flux (Jan. 2017). ....	37
Table 7: RSI calculations–part 2: delta temperature and cumulative temperature (°C) and cumulative heat flux (W/m <sup>2</sup> ). ....	39
Table 8: RSI calculations–part 3: RSI at hourly intervals and convergence factor. ....	41
Table 9: RSI calculation results: summary of results for panel EN1A from January 1–15, 2017. ....	42
Table 10: Vertical variation in temperature distribution in Edmonton and Vancouver. ....	46
Table 11: Comparison between heat flux measured data and calculated heat flux. ....	64
Table 12: Parameters used for WUFI simulations for Moisture Content. ....	73

## List of Figures

Figure 1: Samples of the multi-functional panel layouts: “Type A” (bottom) and “Type B” (top). .....	3
Figure 2: (a) Sample of the materials and (b) application on the interior wall of a commercial building. ....	6
Figure 3: (a) Testing samples and (b) hemp fibres with bicomponent fibres. ....	7
Figure 4: Methodology of the conducted study by (Žigart et al., 2018).....	14
Figure 5: Wall types from “A” to “E” for numerical modelling.....	15
Figure 6: Multi-functional panel “Type A” sample (middle layer of wood fibre and interior/exterior layer of OSB). ....	18
Figure 7: Multi-functional panel “Type B” sample (middle layer of XPS and interior/exterior layer of OSB). ....	19
Figure 8: (a) Representation of the composition and dimensions of “Type A” and “Type B” MFPs; and (b) photograph of the MFP samples. ....	20
Figure 9: Wall assembly composition, “Type A”, “Type B”, and “Type C”. ....	21
Figure 10: (a) Vancouver test hut, and (b) Edmonton test hut.....	22
Figure 11: Layout of the MFPs attached to the test huts. ....	23
Figure 12: Sample of internal wall of the test huts with sensors applied. ....	24
Figure 13: Sensor layout for “Type A” and “Type B” panels. ....	26
Figure 14: Online data acquisition system.....	27
Figure 15: Edmonton test hut equipment: (a) oscillating fan and water pails; (b) under-floor heating control panel, weather station display unit, and laptop connected to data; (c) under- floor heating system; (d) floor temperature display.....	28
Figure 16: Experimental set up in Vancouver: (a) oscillating fan; (b) air conditioning unit; (c) display with indoor conditions; and (d) NaCl added to water pail. ....	29
Figure 17: (a) Weather station installed on the roof of test hut, (b) weather station display installed inside test hut.....	30
Figure 18: Temperature distribution profiles, north and south positioned panels, Edmonton, and Vancouver. ....	47
Figure 19: Average variation of temperature distribution on three vertical levels of the inner wall assembly.....	48

Figure 20: Temperature in various wall layers in Vancouver and Edmonton for three different wall assemblies. ....	51
Figure 21: Hourly temperature profile in the interior layer of the MFPs for Edmonton and Vancouver locations.....	53
Figure 22: Moisture content levels for inner and outer layers of MFPs in Vancouver location...	55
Figure 23 : Moisture content levels for inner and outer layer of MFPs in Edmonton location....	57
Figure 24: Relative humidity and temperature profiles in North and South facing wall assemblies in Edmonton location. ....	59
Figure 25:Relative humidity and temperature profiles, North and South facing wall assemblies in Vancouver location. ....	61
Figure 26: Temperature on the interior surface of MFPs and exterior temperature profiles based on 2 years of data for Vancouver north/south orientations. ....	68
Figure 27:Temperature on the interior surface of MFPs and exterior temperature profiles based on 2 years of data for Edmonton north/south orientations.....	71
Figure 28: RSI calculated for all wall types in January and June, for both locations.....	72
Figure 29: Moisture content comparison between simulated and field results.....	74
Figure 30: Results RSI, All wall assemblies, and locations. ....	76
Figure 31: Moisture content levels for inner and outer layers of MFPs in Edmonton and Vancouver locations.....	78

## **Chapter 1 Introduction**

Canada has extremely cold weather in winter; as such the interest in building solutions for energy savings has been increasing in recent decades. The Canadian residential sector is the third largest energy consumer, accounting for 17% of all energy consumed in the country, where 63% of this consumption results from space heating (NRCan-Office of Energy Efficiency, 2016).

In this regard, various government programs are being implemented in different provinces, some of which include federal regulations. Between April 2007 and March 2012, the EcoENERGY program was adopted into Canada's Economic Action Plan. Notably, the program supported technology and innovation for projects in Aboriginal and Northern communities (NRCan-EcoEnergy, 2014). In Ontario, the ENERGY STAR Multifamily High-rise Pilot program for new construction projects recognizes buildings that are at least 15% more energy-efficient than those that were built following the provincial energy code (ENERGY STAR Program-Canada, 2018).

In addition, another Government of Canada program, Local Energy Efficiency Partnerships (LEEP), helps builders to reduce the time spent seeking out and implementing new technologies for energy savings in their markets through a four-step process: (1) builder planning workshop; (2) technology forum; (3) field trials; and (4) technology publications resulting from builder experiences (NRCan-LEEP, 2019).

The current National Energy Code of Canada for Buildings, NECB 2017, focuses on five key items: (1) building envelope, (2) lighting, (3) heating, ventilating and air conditioning (HVAC) systems, (4) service water heating, and (5) electrical power systems and motors (NRCan-NECB/C, 2017). The research presented in this thesis investigates the thermal performance of two multi-

functional panels (MFPs) to improve the energy efficiency of one of the key items of the NECB: the building envelope.

Professionals worldwide agree that energy efficiency is one of the key factors influencing efforts to achieve sustainable development (Vera & Langlois, 2007). Buildings account for 30% to 40% of the total energy use in North America (UNEP, 2007). Therefore, improvements in the building sector have positive effects on other sectors, notably the power sector, because over half of the electricity consumed today is used in buildings, thus energy-efficient buildings can decrease the necessity of electrical capacity additions in the power sector (IEA, 2017).

In this context, building professionals seek thermally-effective, humidity-resistant, and environmentally-friendly materials. The research presented in this thesis focuses on the investigation of the long-term hygrothermal performance of two innovative and environmentally-friendly MFPs that are attached to the exterior of conventional wall assemblies and are expected to improve the hygrothermal properties of the building envelope in order to reduce the energy consumption of the building.

To ensure that these materials perform effectively, the evaluation involves the calculation of thermal resistance using real-life scenarios in the built test huts in two climatic conditions in Canada: Edmonton, Alberta, with an extremely cold climate, and Vancouver, British Columbia, with a coastal humid climate, as recommended by the ASHRAE-90.1 Standard. This research contributes to the investigation of the hygrothermal performance of two MFPs based on long-term field testing.

## 1.1 Research Objectives

The primary objective of this research is to investigate the hygrothermal performance evaluation results of two types of MFPs for energy-efficient wall assemblies. The MFPs are used as an additional layer attached to the exterior side of conventional wood-frame wall assemblies. The first MFP type, referred to as “Type A”, includes two outer layers of Oriented Strand Board (OSB) 6.4 mm (3/8 in) in thickness and a middle layer of wood-fibre rigid insulation 40 mm (1 9/15 in) in thickness. The second MFP evaluated in this project is referred to as “Type B” and is also composed of 6.4 mm (3/8 in) OSB on the interior and exterior layers but, in this case, the middle insulation layer is 25 mm (1 in) of Extruded Polystyrene (XPS) as illustrated in Figure 1.



Figure 1: Samples of the multi-functional panel layouts: “Type A” (bottom) and “Type B” (top).

This project focused on the field-testing experimentation of the two MFP types at two different locations in Canada: Vancouver and Edmonton. The impact of climatic conditions on the

performance of the panels was investigated through comparisons between data measured from both locations.

For this purpose, two identical demonstration test huts were built, one in Vancouver and one in Edmonton. In each test hut, five wall assemblies were installed along the north- and south-facing orientations, two “Type A”, two “Type B”, and one baseline wall assembly, “Type C”, along each orientation. In this regard, R-values were calculated for the three wall assemblies and results were compared to one another. Measurements from temperature, moisture content, and relative humidity sensors were analyzed in this research. Indoor and outdoor temperature and moisture content profile variations, vertical and horizontal variations on the MFP itself, and comparisons of the results between different panels were also examined.

## **1.2 Organization of Thesis**

Chapter 1 (Introduction) describes the research objective, scope, and structure of the project. Chapter 2 (Literature Review) presents the literature review, starting with an overview of Energy Efficient Buildings, then environmentally-friendly materials for insulation and, to sum up, different methods for hygrothermal evaluation performance are presented. Chapter 3 (Experimental Setup and Implementation) describes the field-testing system, including the materials that are analyzed, sensors types and layout, equipment, indoor conditions, locations and climate conditions, and test hut layouts. Chapter 4 (Hygrothermal Performance Analysis) demonstrates the methodology used to calculate the thermal performance of the MFPs, thermal distribution, thermal bridging, thermal mass results, moisture content levels, and vapour control barrier, as well as a discussion of the results. Chapter 5 (Conclusion) summarizes the results obtained as well as the main contributions; it also considers the limitations of the project and provides recommendations for future work.

## **Chapter 2 Literature Review**

This chapter begins with a review of new technologies and environmentally-friendly materials used to improve the overall efficiency of a building envelope in various climatic conditions. Then, an overview of previous research is presented for methods to evaluate the hygrothermal performance in buildings.

### **2.1 Materials for Building Envelope**

A building can be classified as a high-performance building if it is energy-efficient, durable, and provides comfortable and healthy indoor environment for occupants (Tariku, Kumaran, & Fazio, 2015). Using high-performance materials for the building envelope can increase the energy efficiency of the building. In this manner, the demand for energy-efficient and environmentally-friendly materials for thermal insulation in buildings has increased considerably in recent years.

#### **Environmentally friendly materials**

Binici et al. (2014) tested the use of composites made with sunflower stalk, cotton waste, textile waste, and stubble fibres for thermal insulation. In their study, the researchers combined the agricultural and industrial residues of environmentally-friendly materials in different ratios and tested the thermal performance of the samples in the interior wall of a commercial building as represented in Figure 2. It was found that some of the mixtures were effective insulation materials, classified as 100% organic origin, and could be candidates for commercialization in the future (Binici, Eken, Dolaz, Aksogan, & Kara, 2014).



Figure 2: (a) Sample of the materials and (b) application on the interior wall of a commercial building.

Zhou et al. (2010) investigated the thermal insulation efficiency of Binderless Cotton Stalk Fiberboard (BCSF) and found that it is particularly suitable for use on ceilings as well as for wall applications for energy conservation. BCSF is considered completely environmentally-friendly in the sense that the cotton stalk fibres are bound together using high-frequency hot pressing and no resins or other chemicals are added in the process of fabrication and testing (Xiao-yan Zhou, Zheng, Li, & Lu, 2010).

Panyakaew and Fotios (2011) developed a low-density thermal insulation made from coconut husk and coconut bagasse without the use of chemical binding additives in order to classify the material as fully organic. The researchers used the same technique as (Xiao-yan Zhou et al., 2010), “the hot-pressing method”, to develop a binderless board. The thermal conductivity and density of the boards was compared with other insulation materials as represented Table 1 (Panyakaew & Fotios, 2011).

Table 1: Thermal conductivity of binderless coconut husk insulation board (BCI) and binderless bagasse insulation board (BBI) compared with other insulation materials. (Panyakaew & Fotios, 2011).

Materials	Density (kg/m <sup>3</sup> )	Thermal conductivity (W/mK)	Source
BCI	250-350	0.046-0.068	[4]
BBI	250-350	0.049-0.055	[4]
Kenaf insulation board	150-200	0.051-0.058	[5]
Cotton stalk insulation board	150-450	0.058-0.081	[3]
Cellulose fibres	30-80	0.040-0.045	[6]
Mineral wool (fibreglass and rockwool)	20-200	0.035-0.045	[6]
Polyethylene foam (PE)	50-100	0.035-0.045	[6]
Extruded polystyrene foam (XPS)	25-45	0.030-0.040	[6]
Expanded perlite boards (EPB)	90-490	0.045-0.070	[6]
Vermiculite	70-160	0.046-0.070	[6]

Furthermore, considering the growing demand for green building materials, Korjenic and Petránek (2011) investigated the use of jute, flax, and hemp in combination with shives and a bicomponent fibre binder in six different ratios to develop a new environmentally-friendly insulating material as presented in Figure 3 (Korjenic & Petránek, 2011).



Figure 3: (a) Testing samples and (b) hemp fibres with bicomponent fibres.

(Korjenic & Petránek, 2011).

In their study the insulation material samples were manufactured, and the material characteristics were measured as represented in Table 2. The authors compared the sample properties results with commonly used boards made from different materials (mineral wool, polystyrene, and polyurethane) and concluded that the insulation properties from organic boards are comparable to common insulation boards from other materials.

Table 2: Materials properties of samples.

(Korjenic & Petránek, 2011).

Set of samples	Thickness	Density	Thermal conductivity
	mm	Kg/m <sup>3</sup>	W/mK
1	81.2	26.1	0.0458
2	77.4	32.1	0.0429
3	77.9	30.2	0.0486
4	79.6	29.6	0.0475
5	30.3	33.1	0.0419
6	40.2	82.1	0.0393

Boukhattem et al. (2017) conducted an experimental study on moisture absorption and the effect of humidity on thermal conductivity and density of binderless boards made from date palm fibre (DPF) mesh and a composite based on mortar reinforced with different percentages of date palm fibres ranging from 0% to 51%. The authors tested different techniques and concluded that DPF mesh can be considered a hydrophilic material as it can absorb four times its own weight in water and the addition of DPF to mortar can increase the absorption coefficient of the material significantly. The measured thermal conductivity was 0.033 W/mK, which is comparable to rockwool insulation (Boukhattem, Boumhaout, Hamdi, & Benhamou, 2017).

## **Multi-functional panels (MFPs)**

In recent years, studies exploring new technologies for improving the energy efficiency of buildings increased significantly. In some cases, a combination of materials is prepared to increase the overall performance of the building envelope. The ASTM International defines sandwich panels as a three-layered construction formed by bonding a thin layer (facing) to each side of a thick layer (core). The term “composite” refers to any material in which two or more distinct materials are combined together yet remain uniquely identifiable in the mix. There are a variety of MFPs on the market, such as Composite Structural Insulated Panels (CSIPs), Structural Insulated Panels (SIPs), and Multi-functional panels (MFPs). In all these examples, the panels are a combination of multiple layers of different materials and they are generally employed in the envelope (walls and/or roof) of a building. The various products can be called “composite sandwich panels”. CSIPs can be classified as a variation of SIPs and both combine hygrothermal and structural performance. MFPs are sandwich panels used to improve the overall hygrothermal performance of buildings. They are design to perform both the function of structural sheathing in wood frame construction and provide additional thermal insulation. MFPs are usually applied in retrofit projects as an extra layer of thermal material or to improve the performance of new wall systems.

In 1935, researchers from the Forest Product Laboratory (FPL) designed the first prototype of an SIP in Wisconsin, United States (Panjehpour, Ali, & Lei, 2013). The use of MFPs emerged as a construction technology with the goal to reduce waste and labour. Accordingly, MFPs have become a topic of interest for researchers around the world. As the name suggests, SIPs provide structural performance; in this regard, the structural component of the MFPs has been widely discussed [(Chen, Hao, Chen, & Hernandez, 2015) (Edgars, Kaspars, & Kaspars, 2017), (Mousa

& Uddin, 2012), (Kayello, Ge, Athienitis, & Rao, 2017), (Medina, King, & Zhang, 2008), (Beaudry & MacDougall, 2019)].

Kawasaki and Kawai (2006) investigated the thermal insulation properties of an MFP used as structural insulated walls and floors. The MFP developed was a plywood-faced sandwich panel with a low-density fiberboard core (PSW). The panel was manufactured to improve mechanical properties and the composition of the panels was made from sustainable wood sources. The thickness of the material was 96 mm. Thermal and hygric properties were investigated through laboratory tests and then compared to commercial wood-based boards. Results demonstrate comparable thermal results with already existing materials, but the authors recommend a larger scale study on hygrothermal performance properties in order to analyse other parameters for an energy-efficient building envelope (Kawasaki & Kawai, 2006).

## **2.2 Review on Hygrothermal Performance Evaluation**

At present, reducing energy consumption is of utmost priority worldwide due to environmental and economic concerns (Cruz, Silva, Dias, & Teotónio, 2017). Toward hygrothermal performance evaluation, studies generally include thorough field experimentation[(Aflaki, Mahyuddin, & Baharum, 2016), (Hagerstedt & Arfvidsson, 2010), (Semprini, Marinosci, Ferrante, & Predari, 2016), (Kosny, Fontanini, Shukla, & Fallahi, 2018), (Li, Yu, Sharmin, Awad, & Gül, 2016b)] or modelling and simulations [(Xiaohai Zhou, Derome, & Carmeliet, 2016), (Simko, Krajč, Simko, & Kalús, 2018), (Jang & Kang, 2016),(Stergaard & Svendsen, 2016), (Nik, Mata, Sasic Kalagasidis, & Scartezzini, 2016), (Li, Yu, Sharmin, Awad, & Gül, 2016a)]. Proper design and knowledge of hygrothermal properties of the building envelope are fundamental to achieve an energy-efficient construction (Asdrubali, D'Alessandro, Baldinelli, & Bianchi, 2014) and complete analysis of the material's performance in various climate conditions is crucial to obtain

the expected results. For this reason, building energy performance has been a widely discussed research topic.

Awad et al. (2014) studied the long-term thermal and structural performance of mid-rise (four to six storeys) wood-frame wall systems. Four innovative wall systems were evaluated along with a baseline conventional wall. The wall systems were installed in a full-scale test-house where several sensors were installed in each wall system to measure temperature, heat flow, and relative humidity. The structural performance was tested using full-scale panels in a laboratory setting. A comparison between two engineered-wood I-Joist (TJI 230) wall stud systems, staggered wall stud systems, and a baseline wall system was made, and the researchers found that the I-Joist systems had the highest energy efficiency among the panels; further research on the structural capacity of the I-Joist wall system was recommended (Awad, Gül, Zaman, Yu, & Al-Hussein, 2014).

The thermal performance of a house should be optimized to be considered energy efficient. In this regard, Yang et al. (2016) evaluated a long-term monitoring study on the hygrothermal performance of five wood-frame wall systems using various types of insulation (fiberglass, spray foam, fiberglass with Structural Insulated Sheathing, spray foam with Expanded Polystyrene (EPS) foam rigid insulation, and fiberglass with EPS insulation). In their study, field testing and occupied conditions were applied. The test hut was built in the severe climate condition of Edmonton, Canada, where temperature and relative humidity sensors were affixed to north and west facing walls. The sensors were installed within the wall cavities and the results from the measurements were then analyzed (Li et al., 2016b).

The thermal performance of the panels was calculated first by observing the differences between temperature profiles on inner and outer layers of the wall systems and second by calculating the R-value using the summation technique. The hygric performance was investigated in terms of

humidity ratio evaluations. The four main conditions that lead to mold growth were also analyzed: (1) existence of mold spores; (2) available nutrients; (3) appropriate temperature; and (4) high humidity levels. In conclusion, it was determined that the spray foam panels had the highest thermal efficiency. Also, it was found that the thermal resistance is related to material moisture levels in each layer of the panels, and values decreased as the temperature and humidity ratios increased (Li et al., 2016b).

Sassine (2016) proposed a method based on a complex Fourier series for thermal characterization to determine thermal capacitance and conductivity of the walls in existing buildings; sensors were installed to measure the indoor and outdoor temperature and outdoor heat flux with the data being collected every 20 minutes. The experimental method was compared with laboratory results and the accuracy of the method was considered satisfactory (Sassine, 2016).

Mundt et al. (2015) investigated the hygrothermal performance of wood-frame roofs in the cold climate of Northern European countries. The authors compared simulated results with real calculations for two types of roof design: (1) cold roof with a ventilated air gap located under the tongued and grooved wooden roof boarding; and (2) ventilated cold attics under the tongued and grooved wooden roof boarding. In both cases the software used for the simulations was WUFI and the field data calculations were made with results provided from measurements for relative humidity and temperature sensors. The results demonstrate a strong similarity between calculated and simulated results (Mundt Petersen & Harderup, 2015).

Ge and Baba (2015) investigated the impact of thermal bridging on a two-storey low-rise residential building. Three modelling methods (Direct 3D dynamic modelling method, Equivalent wall method, and Equivalent U-value method) were used to evaluate the energy performance of the building and the results were compared. The authors used WUFI plus software and the

simulations were conducted in two climate conditions, Quebec City (Zone 7) and Phoenix (Zone 2B). In the cold climate (Zone 7), results from simulations using the three methods was as high as 13 % and in the warm climate (Zone 2B) the thermal bridge increased the annual cooling load by 20%; the difference between methods was 6% (Ge & Baba, 2015).

Zigart et al. (2018) investigated the environmental impact of four types of building envelope systems commonly used in low rise buildings in Slovenia and other Central-European countries. The building envelope types evaluated were reinforced concrete, brick, cross-laminated timber, and timber-frame panels. The authors first compared building components (walls and roofs) with different structural systems and then they exchanged the thermal insulation for environmentally-friendly alternatives as represented in Figure 4. It was concluded that timber-framed construction has the best overall environmental performance, followed by the cross-laminated timber system. In regard to insulation alternatives, rockwool insulation presented the worst environmental results followed by EPS insulation and wood fibre insulation. It is important to note that the assessment was made for low-rise buildings (Žigart, Kovačič Lukman, & Premrov, 2018).

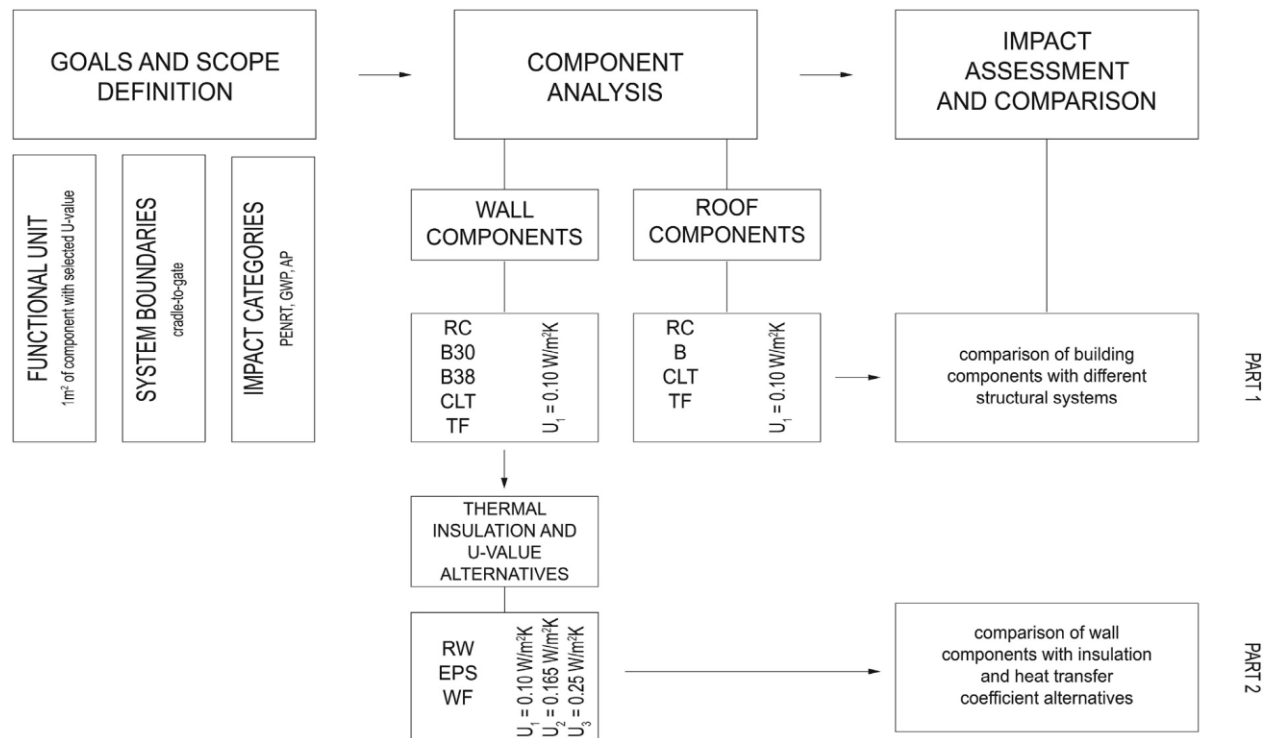


Figure 4: Methodology of the conducted study by (Žigart et al., 2018)

A study conducted by Winkler, Nore, and Antretter (2014) examined the moisture buffering (the ability of the materials within a room to moderate variations in the relative humidity) and latent heat exchange of wooden surfaces. They used simulation models to evaluate the whole hygrothermal performance of the building. The simulations were carried out for both a long-term and short-term basis. The study concluded that wooden materials have the ability to reduce the fluctuation of relative humidity within a building (Winkler, Nore, & Antretter, 2014).

Djamila et al. (2018) analyzed the energy-efficiency of building envelopes in the hot, humid climates of Asian countries. The researchers compared the results from heat transfer through the building envelope in Malaysia and Singapore to the American and European standards. The authors addressed the main issues found when comparing energy codes and developed an experimental model to be used in Asian markets, including some recommendations for future studies (Djamila, Rajin, & Rizalman, 2018).

The energy performance of building envelopes made with organic materials was investigated by (Biks, Ratushnyak, & Ratushnyak, 2019). In their study, the “thermal inertia” investigated also by (Verbeke & Audenaert, 2018), (Wang, Bras, Sivandran, & Knox, 2010) of the building systems was used to quantify the heat loss through the building envelope over a period of time. The environmental wall systems chosen by the authors included hempcrete, adobe, straw bale panel, earthbag, and cordwood masonry as described in Figure 5. It was concluded that when comparing the wall systems, the hempcrete demonstrated better performance and the earthbags had the least favorable performance among the five analyzed assemblies.

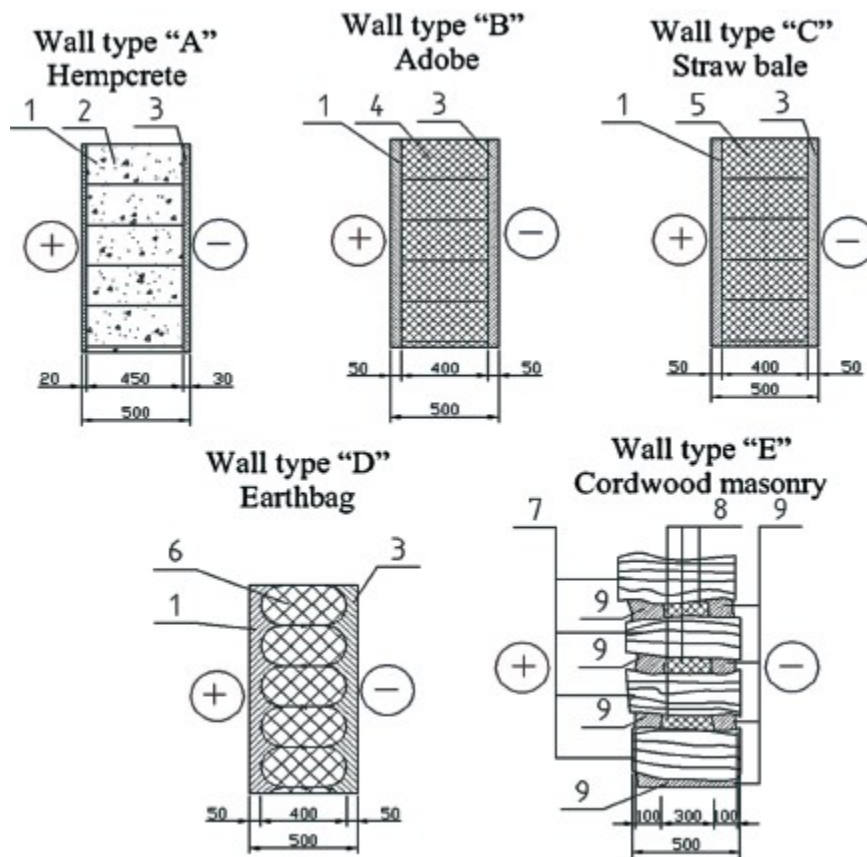


Figure 5: Wall types from “A” to “E” for numerical modelling.

(1: internal lime-sand plaster; 2: hemp concrete; 3: external lime-sand plaster; 4: adobe blocks; 5: straw bales; 6: bags with soil; 7: cordwood; 8: insulation (chopped straw); 9: lime-sand plaster) (Biks et al., 2019).

Hernández-pérez et al. (2018) investigated the impact of three different roof coatings on the overall thermal performance of a building. The coatings were applied to a concrete slab roof and then compared to a baseline roof with no coating. The study was based on field experimentation using mobile outdoor test cells. The roofs were tested for two weeks and then the authors used the field data to conduct simulations for a period of one year. It was found that roofs with white coating yielded superior thermal results, followed by grey coating, and finally red coating. In the same study, the cost effectiveness of the roof coatings was evaluated and it was found that the use of the white coating on roofs in the warm climate of Mexico will greatly reduce the energy consumption of the building with a payback period of less than two years (Hernández-pérez, Xamán, Macías-melo, & Aguilar-castro, 2018).

Several studies also conducted economic or environmental investigations using the life cycle assessment (LCA) technique (Radon, Pisello, Castaldo, & Piselli, 2016), (Manyumbu, Martin, & Fransson, 2016), (Gounni, Mabrouk, El Wazna, & Kheiri, 2019), (Wang, Ploskić, Song, & Holmberg, 2016), (Lawania & Biswas, 2016). Azari et al. (2016) evaluated the environmental impacts on a low-rise building in Seattle, Washington. The authors made adjustments to the insulation type, window frame material, and overall R-value of the wall assemblies and compared them with the total impact on the efficiency of the building and consequently the environmental impact (Azari, Garshasbi, Amini, Rashed-Ali, & Mohammadi, 2016).

Asdrubali and Baldinelli (2011) evaluated six case studies of thermal transmittance in green building masonries from field measurements where these buildings were designed with bio-architectural solutions. The authors then compared in situ thermal transmittance measurements with the calculated results. Findings of this study demonstrated that the in situ thermal transmittance and U-value differ from the expected results. In this regard the authors suggested

that highly efficient buildings should always have field measurement results to be validated as energy efficient (Asdrubali & Baldinelli, 2011), (Bienvenido-Huertas, Moyano, Marín, & Fresco-Contreras, 2019).

Ge et al. (2017) investigated the hygrothermal performance of attic ventilation systems through the evaluation of three types of houses in the cold northern-Canadian regions of Nunavik (in northern Quebec) and Nunavut. All the buildings evaluated were duplexes, two of which had ventilated attics with differing filter membrane designs and the third house was constructed using SIPs and had no attic ventilation. Moisture content, temperature, and relative humidity sensors were used to evaluate the performance of the attics in the extreme cold conditions. The authors found that attic ventilation was extremely important in order to avoid condensation in the buildings (Ge, Wang, & Baril, 2017).

As previously mentioned, the energy efficiency of buildings is a widely discussed topic and new technologies are continually emerging. As such, the research presented in this thesis focuses on the field monitoring testing of two types of MFPs that can be used in the construction of new buildings or in the retrofit of existing buildings to improve the overall hygrothermal performance of the building envelope.

## Chapter 3 Experimental Setup and Implementation

In this chapter, the experimental setup and implementation is described in detail. In this regard, the MFP design, test hut layout, sensor types and implementation, indoor conditions in the test hut, and the climates chosen for this evaluation are presented.

### 3.1 Multi-functional Panels (MFPs)

In this project, two types of MFPs designed to achieve high energy-efficiency requirements in buildings were evaluated. The “Type A” wall assembly is a combination of interior and exterior layers of Aspen OSB, with a thickness of 6.4 mm (1/4 in) and a middle layer of European wood-fibre rigid insulation with a thickness of 40 mm (1-9/16 in) (Gutex Multitherm, by GUTEX Holzfaserplattenwerk, Germany) as presented in Figure 6.



Figure 6: Multi-functional panel “Type A” sample (middle layer of wood fibre and interior/exterior layer of OSB).

A thickness of 40 mm was chosen for the wood fibre in order to achieve an R-5 of thermal resistance as recommended in the product specifications. The wood fibre rigid insulation applied in the fabrication of the MFP is an environmentally-friendly and fully-recyclable material.

The “Type B” wall assembly, as presented in Figure 7, also includes both interior and exterior layers of Aspen OSB with a thickness of 6.4 mm (1/4 in), but the middle layer is extruded polystyrene rigid foam insulation (XPS) with a thickness of 25 mm (1 in) (by Owens Corning Formular). In order to have comparable products, the thickness chosen for the “Type B” MFP was 25 mm to achieve an R-5 of thermal resistance as described in the XPS product specifications.



Figure 7: Multi-functional panel “Type B” sample (middle layer of XPS and interior/exterior layer of OSB).

Both MFPs are glued with Purbond HB E452 polyurethane adhesive (Purbond AG, Switzerland) and are designed to be attached to the outer side of conventional wood-frame walls or roofs in order to provide additional R-5 insulation. In this study, the MFPs were attached to the exterior of the wood-frame walls. Figure 8(a) demonstrates the composition and dimensions of the proposed MFPs and Figure 8(b) presents a photograph of the MFP samples.

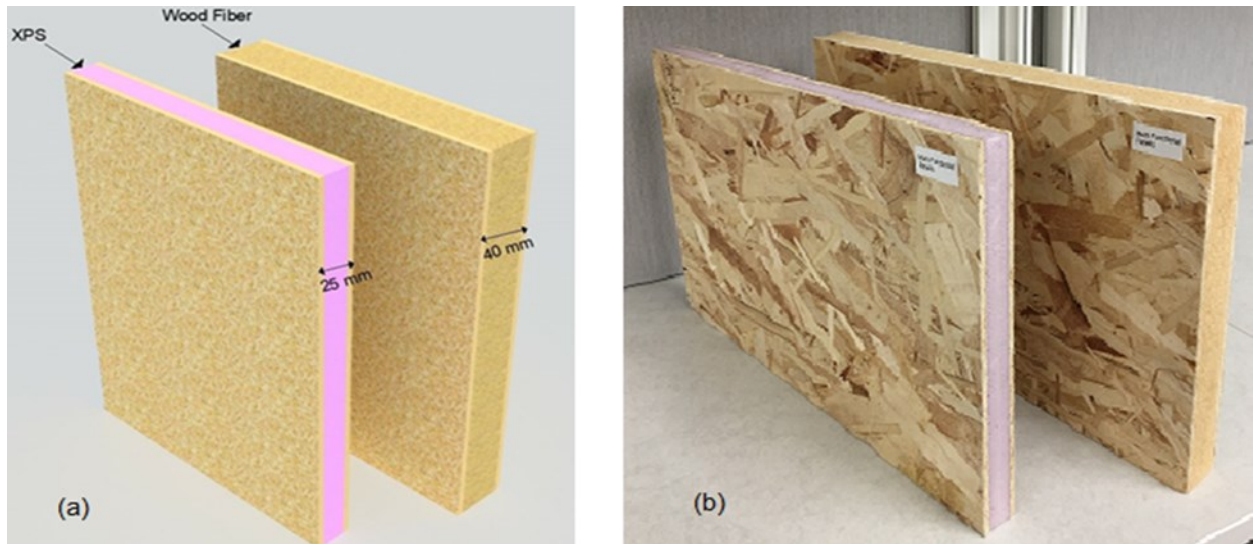


Figure 8: (a) Representation of the composition and dimensions of “Type A” and “Type B” MFPs; and (b) photograph of the MFP samples.

To evaluate the performance of the MFPs, a panel called “Type C” comprising a conventional wall assembly was also included in this study. Panel “Type C” was used as a baseline for this research.

Figure 9 summarizes the wall composition of the 3 types of wall assemblies: “Type A”, “Type B”, and “Type C”.

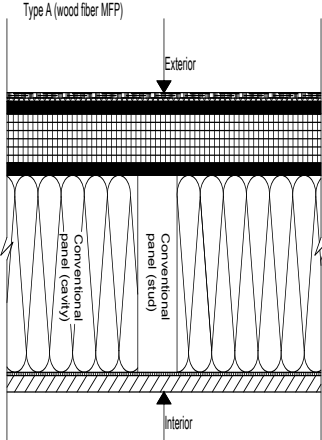
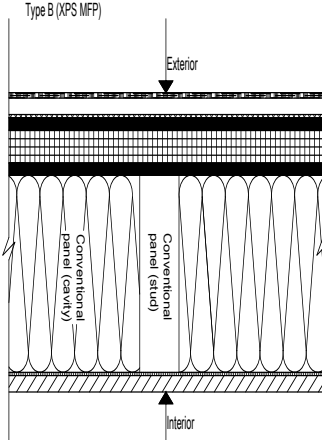
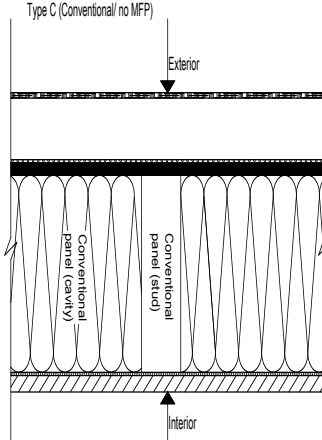
“Type A” assembly	“Type B” assembly	“Type C” assembly
		
Interior to exterior wall components		
<ul style="list-style-type: none"> <li>• 12.5 mm (1/2 in.) Interior Gypsum Board</li> <li>• 0.15 mm Polyethylene</li> <li>• 140 mm (5 ½ in.) Fiber Glass</li> <li>• 6.4 mm (3/8 in.) OSB Sheathing</li> <li>• 40 mm (1 9/15 in.) Wood Fibre Insulation</li> <li>• 6.4 mm (3/8 in.) OSB Sheathing</li> <li>• 20 mm (3/4 in.) Air Cavity</li> <li>• 4.76 mm (3/16 in.) Vinyl Siding</li> </ul>	<ul style="list-style-type: none"> <li>• 12.5 mm (1/2 in.) Interior Gypsum Board</li> <li>• 0.15 mm Polyethylene</li> <li>• 140 mm (5 ½ in.) Fiber Glass</li> <li>• 6.4 mm (3/8 in.) OSB Sheathing</li> <li>• 25 mm (1 in.) Extruded Polystyrene Insulation (XPS)</li> <li>• 6.4 mm (3/8 in.) OSB Sheathing</li> <li>• 20 mm (3/4 in.) Air Cavity</li> <li>• 4.76 mm (3/16 in.) Vinyl Siding</li> </ul>	<ul style="list-style-type: none"> <li>• 12.5 mm (1/2 in.) Interior Gypsum Board</li> <li>• 0.15 mm Polyethylene</li> <li>• 140 mm (5 ½ in.) Fiber Glass</li> <li>• 12.5 mm (1/2 in.) OSB Sheathing</li> <li>• 20 mm (3/4 in.) Air Cavity</li> <li>• 4.76 mm (3/16 in.) Vinyl Siding</li> </ul>

Figure 9: Wall assembly composition, “Type A”, “Type B”, and “Type C”.

### 3.2 Test Huts

To evaluate the hygrothermal performance of the two MFPs in an actual situation, two identical test huts were built in different climates. To evaluate the performance of the MFPs in different climatic conditions, the first unit was built in the humid coastal climate of Vancouver, as represented in Figure 10(a). On the other hand, the MFPs were designed to perform in climates with extreme temperatures. In this regard, the other test hut was built in Edmonton, which

experiences average temperatures below 0°C five months per year, between November and March, as presented in Figure 10(b).



Figure 10: (a) Vancouver test hut, and (b) Edmonton test hut.

The demonstration buildings are 6.10 m (20 ft) long and 2.44 m (8 ft) wide and were built with conventional wood-frame wall assemblies; the two MFP types were then attached to the exterior side of these wall assemblies. The test huts are each equipped with eight panels with MFPs (four panels with wood fibre composition and four panels with XPS composition) attached to the exterior side; two baseline panels are affixed in the middle of each wall. The test hut layout and wall panel configuration are presented in Figure 11.

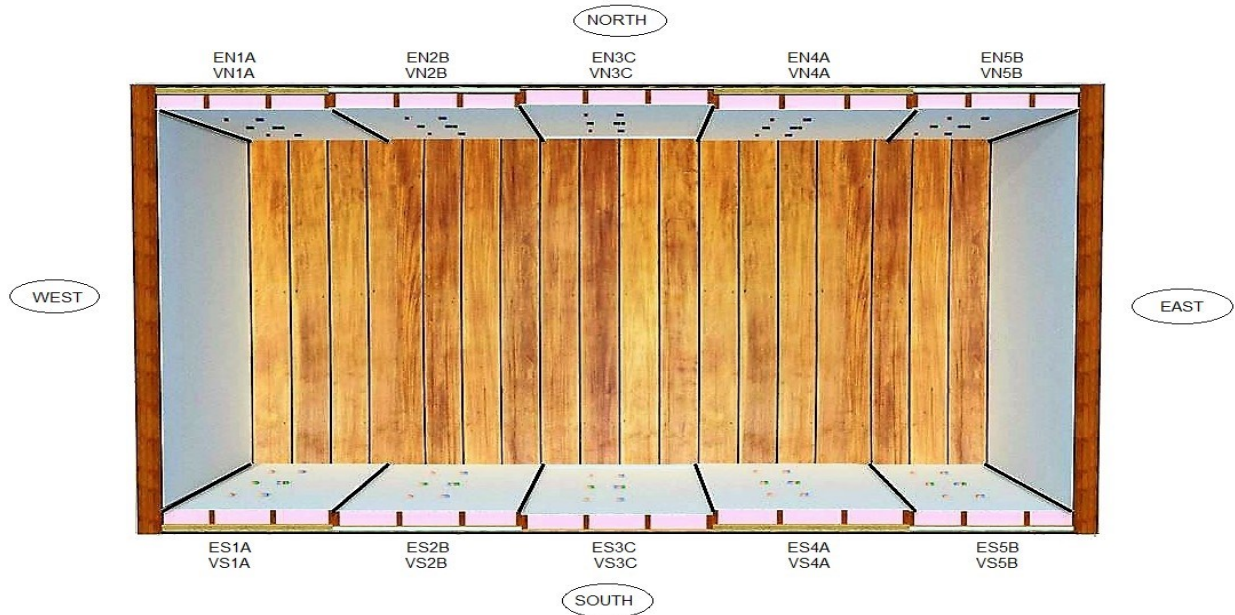


Figure 11: Layout of the MFPs attached to the test huts.

North- and south-facing walls are divided into five panels: two “Type A”, two “Type B”, and one “Type C” with no MFP are attached to the exterior side of the test hut walls. The labelling of the panels defines their location (E for Edmonton and V for Vancouver), orientation (N for north and S for south), position within the same wall (1 to 5 from west to east), and panel type (A for wood fibre, B for XPS, and C for conventional wall assembly).

### 3.3 Sensor Types and Layout

In order to evaluate the hygrothermal performance of the MFPs, nearly 200 sensors were installed in each test hut: 132 independent temperature sensors, 176 point moisture measurement (PMM) with temperature sensors, 30 cavity relative humidity and temperature sensors, 40 heat flux sensors, and 8 long pin sets; finally, a weather station was installed in each test hut as summarized in Table 3.

Table 3: Sensor type and quantity used in experimental setup.

Sensor Type	Qty in each test house	Total
Independent temperature sensors	66	132
PMM, point moisture measurement (with temperature sensor)	88	176
Cavity relative humidity & temperature	15	30
Heat flux	20	40
Long pin sets	4	8
Weather station	1	2

Furthermore, to conduct an analysis of the material performances, sensors were installed in specific locations in the demonstrational buildings. Figure 12 presents a photograph of the sensors installed on the interior side of the walls at the test hut in Edmonton.



Figure 12: Sample of internal wall of the test huts with sensors applied.

Figure 13 presents the sensor layout configuration of the wall assemblies under investigation. Moisture content sensors (represented by blue squares in Figure 13) integrated with thermocouples (represented by red squares in Figure 13) were installed on each side of the MFPs (“Type A” and “Type B”) and on the interior surface of the wall systems. For “Type C”, moisture content sensors integrated with thermocouples were installed on the exterior and interior layers of the wall assembly. These moisture content sensors, along with the thermocouples, were installed at three

vertical levels along the height of each test hut. The lower, middle, and upper levels were set at 0.6 m (2 ft), 1.2 m (4 ft), and 1.8 m (6 ft). Several factors such as air temperature, air pressure, and material properties can affect the air movement and moisture measurement within the wall assembly.

Moreover, to facilitate the hygrothermal analysis, the moisture content and temperature were measured continuously at different levels and exposed to natural outdoor conditions. Individual temperature sensors (red squares) were placed across the MFP and typical wood-frame wall. Temperature sensors were also placed on the exterior and interior layers of the studs. The individual temperature sensors were also placed in three vertical levels of the test hut. Six humidity sensors (yellow squares) integrated with temperature sensors (red squares) were installed to measure the indoor relative humidity and temperature at two different levels along the longer axis of each test hut. The relative humidity and temperature were also measured inside the cavity of each of the panels. To calculate the R-value of the proposed wall assemblies, heat flux sensors (green squares) were installed on the interior surfaces of the cavity and stud of each panel.

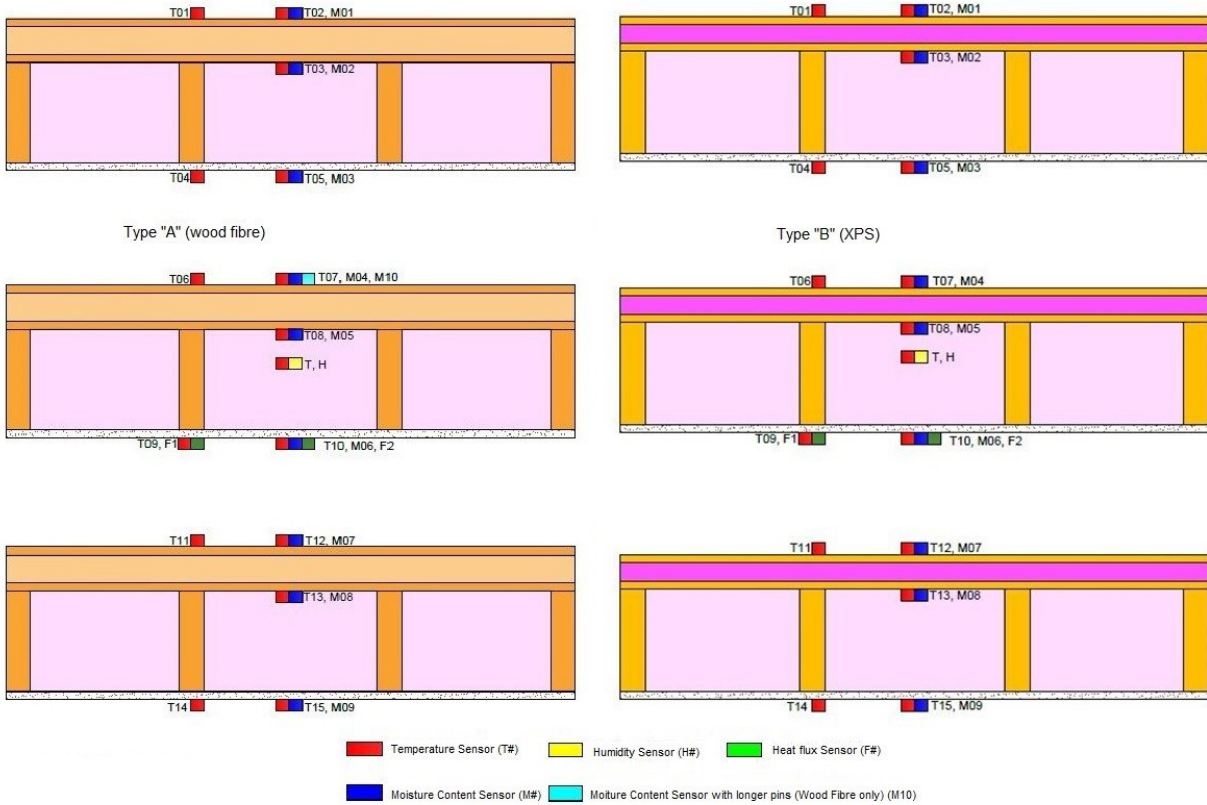


Figure 13: Sensor layout for “Type A” and “Type B” panels.

During the testing period, the data was collected using an online data acquisition system, as presented in Figure 14. The data collection began in June 2015 and August 2015 for Vancouver and Edmonton test huts, respectively, and ended in March 2018 for both test huts. The monitored data was collected at 15-minute intervals and is stored in an online database. Data was collected for over two years; however, occasional sensor malfunctions were incurred at some points of the data collection process resulting in missing data.

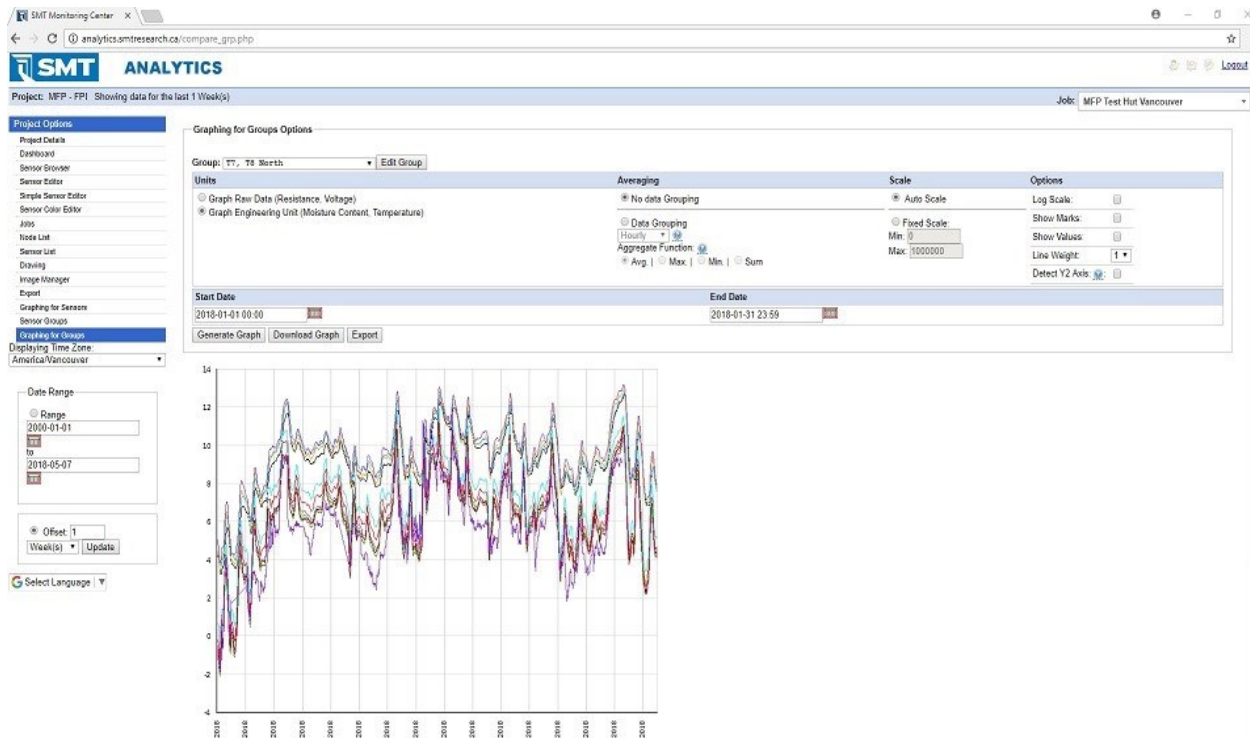


Figure 14: Online data acquisition system.

### 3.4 Indoor Ambient Conditions

The demonstration buildings were equipped with an under-floor heating system, an air conditioning unit, and a 12-in pedestal fan to maintain constant indoor conditions as recommended by the American Society of Testing and Materials (ASTM). The air conditioning unit was set to 22°C as was the under-floor heating system. An oscillating 12-in fan was positioned in the opposite corner from the door to circulate the air uniformly. To maintain acceptable indoor relative humidity levels, two five-gallon water pails were placed in the middle of each test hut. Figure 15 presents the indoor equipment for the test hut located in Edmonton.



(a)



(b)



(c)



(d)

Figure 15: Edmonton test hut equipment: (a) oscillating fan and water pails; (b) under-floor heating control panel, weather station display unit, and laptop connected to data; (c) under-floor heating system; (d) floor temperature display.

In the Vancouver test hut, a saturated salt solution (NaCl) was added to the water to provide moisture and desiccant to the indoor environment. On the other hand, in Edmonton no NaCl solution was necessary, but an additional pail of water was added due the low relative humidity levels, especially in winter months. Figure 16 presents photographs of the Vancouver test hut.



Figure 16: Experimental set up in Vancouver: (a) oscillating fan; (b) air conditioning unit; (c) display with indoor conditions; and (d) NaCl added to water pail.

### 3.5 Location and Climate Conditions

In order to monitor the meteorological conditions, a weather station was installed on the rooftop of each test hut and a display monitor connected to the weather station was installed inside each

test hut as illustrated in Figure 17(a) and Figure 17(b), respectively. The weather stations collect information such as relative humidity, temperature, wind speed and direction, precipitation, solar radiation, and atmospheric pressure.



(a)



(b)

Figure 17: (a) Weather station installed on the roof of test hut, (b) weather station display installed inside test hut.

Table 4 summarizes the monthly weather statistics for Edmonton where the temperature varies between  $-29.23^{\circ}\text{C}$  and  $31.38^{\circ}\text{C}$  with an average of  $1.95^{\circ}\text{C}$  and standard deviation of  $11.73^{\circ}\text{C}$ . The average outdoor relative humidity is 71.13% with a standard deviation of 17.47%. Edmonton is also considered to be a dry climate with an average daily rainfall of 0.31 mm.

Table 4: Edmonton weather statistics.

		Temperature (°C)	Dew point (°C)	Wind Speed (km/h)	Outside RH	Solar Radiation (W/m <sup>2</sup> )	Pressure hPa	Daily rain (mm)
2015	Nov	-5.47	-10.04	4.88	71.96	36.95	1020.84	0.01
	Dec	-7.67	-10.29	4.45	82.31	23.42	1010.24	0.00
2016	Jan	-8.27	-11.28	4.49	80.05	34.73	1014.99	0.07
	Feb	-1.42	-6.14	6.08	72.19	67.01	1014.29	0.05
	Mar	2.37	-2.88	6.37	71.40	115.66	1009.50	0.12
	Apr	8.92	-1.25	8.66	53.89	181.02	1013.25	0.11
	May	12.84	2.27	7.20	55.86	211.00	1010.95	1.27
	Jun	18.95	8.27	7.14	53.62	260.77	1005.78	0.40
	Aug	15.32	9.90	7.12	71.87	180.16	1013.82	0.27
	Sep	12.12	5.37	6.44	66.51	136.00	1012.11	0.17
	Oct	2.57	-0.13	5.30	83.38	61.72	1012.56	0.38
	Nov	1.81	-1.83	5.26	79.36	29.50	1010.90	0.14
	Dec	-9.94	-14.20	6.74	73.70	26.26	1017.87	0.01
	2017	Jan	-7.59	-11.05	5.19	77.68	32.96	1015.93
Feb		-6.34	-10.44	5.14	74.25	61.98	1012.42	0.12
Mar		-4.45	-8.18	6.62	76.68	127.50	1016.01	0.10
Apr		3.60	-0.45	6.50	77.22	133.10	1014.01	0.65
May		14.09	3.60	7.70	53.54	226.57	1011.34	0.73
Jun		16.52	8.19	8.26	61.28	247.09	1010.56	0.68
Jul		19.03	11.93	6.27	65.83	233.42	1014.34	0.53
Aug		17.34	10.11	5.08	65.43	196.56	1016.32	0.97
Sep		13.18	6.15	6.62	66.17	135.85	1014.03	1.10
Oct		5.35	-0.87	7.59	66.58	71.85	1013.26	0.24
Nov		-6.69	-9.41	5.69	81.58	37.58	1014.04	0.13
Dec		-7.15	-12.04	6.34	70.05	29.72	1023.70	0.03
2018	Jan	-9.36	-12.48	5.46	78.85	36.51	1018.03	0.02
	Feb	-11.91	-16.22	6.11	71.85	79.47	1019.64	0.09
	Mar	-4.81	-8.36	6.26	77.45	129.36	1016.87	0.10
	Average	1.95	-3.47	6.25	71.13	108.84	1014.30	0.31
	Max	31.38	18.88	38.23	97.00	1011.75	1048.90	51.60
Min	-29.23	-32.50	0.00	9.75	0.00	980.93	0.00	
StdDev	11.73	9.52	4.77	17.47	187.95	10.16	1.86	

For the Vancouver location, the monthly weather statistics are presented in Table 5. The temperature varies between a minimum and maximum of -6.40°C and 32.53°C, respectively, with

an average of 10.92°C and a standard deviation of 6.38°C. The average daily rainfall in Vancouver is 1.66 mm, which is 5.3 times higher than that of Edmonton. The average outdoor relative humidity in Vancouver is 81.05% with a standard deviation of 13.05%.

Table 5: Vancouver weather statistics.

	Vancouver	Temperature (°C)	Dew point (°C)	Wind Speed (km/h)	Outside RH	Solar Radiation (W/m <sup>2</sup> )	Pressure hPa	Daily rain (mm)
2015	Jun	18.70	12.01	2.65	66.69	281.71	1016.25	0.13
	Jul	21.47	12.91	2.10	59.83	296.55	1016.73	0.00
	Aug	18.66	13.65	2.39	73.93	195.51	1013.98	1.18
	Sep	14.23	11.11	2.33	82.11	140.04	1015.22	0.75
	Oct	12.55	10.48	1.84	87.67	74.81	1015.48	1.84
	Nov	5.78	3.85	2.14	87.73	44.72	1017.82	2.58
	Dec	5.31	3.86	3.28	90.49	21.95	1009.45	3.76
2016	Jan	5.60	4.48	2.37	92.39	30.81	1011.86	2.58
	Feb	7.22	5.42	2.21	88.60	56.49	1018.92	1.89
	Mar	8.52	5.40	2.95	81.96	111.30	1011.93	2.17
	Apr	12.57	7.95	2.49	75.01	187.11	1017.16	0.35
	May	14.84	9.10	2.57	70.63	223.03	1015.94	0.99
	Jun	16.18	11.46	2.47	74.90	230.03	1017.24	1.14
	Jul	18.11	14.03	2.33	77.78	232.88	1016.82	0.96
	Aug	18.91	13.97	2.20	74.55	214.81	1015.31	0.15
	Sep	14.43	11.31	2.30	82.13	147.33	1018.36	0.91
	Oct	10.90	8.92	2.67	88.00	56.42	1009.70	2.59
	Nov	9.25	7.56	2.67	89.42	25.94	1012.27	3.30
	Dec	1.28	-0.48	1.99	88.40	26.54	1019.12	2.26
2017	Jan	2.67	-0.53	2.17	80.94	38.40	1016.10	1.36
	Feb	3.44	0.91	2.13	84.86	63.47	1010.55	1.87
	Mar	6.34	4.50	2.69	88.32	75.92	1014.70	3.00
	Apr	9.19	6.34	2.94	83.03	146.51	1014.00	2.54
	May	13.40	8.93	2.33	76.03	213.66	1015.82	1.71
	Jun	16.15	10.69	2.03	71.81	239.11	1015.55	0.79
	Jul	18.69	12.79	2.39	69.52	273.67	1017.67	0.05
	Aug	19.64	14.23	1.92	71.77	219.64	1015.36	0.00
	Sep	16.87	11.60	1.71	72.67	144.09	1014.16	0.65
	Oct	10.35	7.17	1.82	81.11	91.77	1018.06	1.83
	Nov	6.65	4.15	2.45	84.36	29.24	1011.55	3.09
	Dec	3.17	1.24	1.42	87.11	26.74	1024.59	1.99
2018	Jan	5.62	4.14	2.64	90.02	22.93	1014.97	3.25
	Feb	1.41	-1.05	2.63	84.13	78.40	1017.94	1.27
	Mar	6.48	3.51	2.06	82.01	116.05	1015.12	1.77
	Average	10.92	7.53	2.33	81.05	125.29	1015.39	1.66
	Max	32.53	18.75	17.70	99.00	1011.25	1039.20	50.03
	Min	-6.40	-13.63	0.00	20.75	0.00	133.90	0.00
	StdDev	6.38	5.14	1.96	13.05	221.89	9.77	4.15

## Chapter 4 Hygrothermal Performance Analysis

To understand the long-term effects on the performance of the building envelope, in this chapter, the wall systems under investigation are analyzed based on several criteria such as the type of material, geographical location, and sensor measurements (i.e., moisture content, temperature, and relative humidity). The results for each wall assembly are then discussed and compared at the end of the chapter.

### 4.1 Calculation of the Thermal Resistance from the Field Data

The thermal analysis component of this project was carried out by monitoring the long-term temperature and heat flux performances of each wall assembly type. Following the standard practice for determining the thermal resistance of building envelope components from in-situ data, the ASTM-C1155-95/2013 guide was selected to calculate the R-values in this study. The standard recommends two different techniques to compute the thermal resistance, the summation technique and the least squares technique. The summation technique was selected in order to determine the thermal resistance of the wall system in terms of R-values. The first step of this method was to calculate the difference between indoor and outdoor surface temperatures of each wall system using Eq. 1:

$$\Delta T_s = T_{is} - T_{os} \quad (1)$$

where  $\Delta T_s$  represents the temperature difference for the surface;  $T_{is}$  represents the indoor surface temperature; and  $T_{os}$  represents the outdoor surface temperature. The data was collected in intervals of 15 minutes and then grouped into 1-hour intervals to follow the recommendation of the standard (ASTM – C1155-95/2013). The thermal performance was calculated using Eq. 2:

$$R_e = \frac{\sum_{k=1}^M \Delta T_s k}{\sum_{k=1}^M q_k} \quad (2)$$

where  $R_e$  represents the estimated thermal resistance (RSI) in  $\text{m}^2\cdot\text{K}/\text{W}$ ;  $k$  represents the counter for summation of times series data;  $M$  indicates the test duration for each convergence in hours; and  $q$  represents the heat flux in  $\text{W}/\text{m}^2$ . Based on the cumulative difference in temperature and heat flux for each wall, an hourly thermal resistance was calculated using Eq. 2. The RSI calculations are based on 12-hour intervals where, in order to achieve the stability over time, Eq. 3 was applied:

$$CR_n = \frac{R_e(t) - R_e(t - n)}{R_e(t)} \quad (3)$$

where  $CR_n$  represents the convergence factor;  $R_e$  indicates the thermal resistance; and  $t$  denotes the time in hours. The thermal measurement results and the RSI calculation results were collected and graphs were performed for each panel. Following the determination of the convergence factor, the consistency of the convergence factor to remain below a chosen value for at least three periods of length,  $n$ , was measured, where  $CR_n$  is required to be below 10%. In order to test the consistency of the convergence factor, the variance of R-values was calculated using Eq. 4 as follows:

$$V(R_e) = [S(R_e)/\text{mean}(R_e)] \times (100\%) \quad (4)$$

where  $V(R_e)$  denotes the coefficient of variation of the estimated thermal resistance;  $S(R_e)$  represents the standard deviation of the estimated thermal resistance; and three values of  $R_e$  were taken for the variation calculation.

In order to calculate the R-value of the wall assemblies using the summation technique, data from five temperature sensors and two heat flux sensors for each panel was included in the calculations. The temperature sensors T06 and T09 were attached to the stud, T06 to the exterior and T09 to the interior. The heat flux sensor F1 was attached to the interior layer beside the temperature sensor T09. For the wall cavity, the temperature sensor T07 was attached to the exterior layer, T08 in the middle layer after passing through the MFP, and T10 to the interior layer. The heat flux sensor F2

was positioned beside T10 in the interior layer of the wall cavity. Results from the calculation are presented in the discussion section of this chapter.

Sample data from the panel EN1A (Edmonton, north, position 1, MFP “Type A”) used for the calculation is presented in Table 6.

Table 6: RSI calculations—part 1: sample time series raw data as temperature and heat flux (Jan. 2017).

DATA - January/2017 (Panel EN1A)							
DateTime	Temperature (°C)					Heat Flux (W/m <sup>2</sup> )	
	T06	T07	T08	T09	T10	F1	F2
01-0:00	-6.30	-6.51	-0.49	17.07	17.47	11.25	6.52
01-1:00	-6.36	-6.62	-0.77	16.96	17.39	10.68	6.21
01-2:00	-6.36	-6.64	-0.97	16.83	17.26	11.07	5.77
01-3:00	-6.28	-6.54	-1.11	16.76	17.18	10.97	5.94
01-4:00	-6.32	-6.53	-1.19	16.68	17.10	11.91	6.92
01-5:00	-6.51	-6.69	-1.25	16.61	17.07	12.11	6.23
01-6:00	-6.63	-6.82	-1.34	16.50	16.95	12.09	6.13
01-7:00	-6.74	-6.93	-1.44	16.45	16.91	11.53	6.28
01-8:00	-6.80	-6.97	-1.53	16.63	17.11	10.57	5.92
01-9:00	-6.77	-6.95	-1.58	17.39	17.95	13.86	8.68
01-10:00	-6.49	-6.64	-1.54	18.14	18.78	16.57	9.81
01-11:00	-6.41	-6.58	-1.38	18.57	19.23	18.23	9.97
01-12:00	-6.06	-6.16	-1.21	18.63	19.25	14.22	7.44
01-13:00	-5.88	-5.97	-1.00	18.85	19.48	13.48	7.16
01-14:00	-6.22	-6.33	-0.81	19.18	19.79	14.32	8.32
01-15:00	-6.92	-7.07	-0.77	19.34	19.94	15.02	7.70
01-16:00	-8.32	-8.69	-0.97	19.15	19.73	15.28	7.88
01-17:00	-9.87	-10.64	-1.57	18.34	18.83	10.25	4.43
01-18:00	-11.44	-12.37	-2.54	17.50	17.89	9.00	3.55
01-19:00	-11.69	-12.49	-3.64	17.08	17.46	9.13	4.77
01-20:00	-12.07	-12.93	-4.44	16.87	17.29	11.40	6.90
01-21:00	-11.57	-12.14	-5.03	16.39	16.79	9.59	4.73
01-22:00	-10.93	-11.48	-5.26	16.24	16.70	10.78	6.38
01-23:00	-11.18	-11.82	-5.26	15.91	16.39	11.93	5.62
02-1:00	-13.28	-14.31	-5.69	15.57	16.07	12.60	6.46
02-2:00	-14.29	-15.16	-6.35	15.53	16.06	11.89	6.61
02-3:00	-14.80	-15.81	-7.02	15.37	15.89	11.93	6.00
02-4:00	-15.58	-16.58	-7.65	15.20	15.71	12.69	6.52
02-5:00	-16.63	-17.76	-8.29	15.04	15.57	12.83	6.34
02-6:00	-17.56	-18.72	-9.01	14.94	15.49	12.97	6.85
02-7:00	-18.60	-19.79	-9.78	14.65	15.18	12.77	6.62
02-8:00	-19.31	-20.48	-10.56	14.45	15.01	13.94	8.01
02-9:00	-19.67	-20.75	-11.28	14.37	14.94	13.30	7.36
02-10:00	-18.69	-19.39	-11.80	14.22	14.80	14.37	7.42
02-11:00	-16.22	-16.61	-11.74	13.93	14.56	13.07	6.85
02-12:00	-14.58	-14.86	-11.01	13.84	14.44	14.59	7.82

Table 7 presents a sample of the first part of the calculation using summation technique where the data collected from temperature sensors was applied to determine the delta temperature and cumulative temperature in the stud (temperature sensors T06 and T09), the wall cavity (temperature sensors T07 and T10), the MFP (temperature sensors T07 and T08), the wall assembly (temperature sensors T08 and T10), and the cumulative heat flux calculation with the data collected from sensors F1 and F2. In this study the calculations were conducted bi-weekly and the results were summarized after two years of data was collected.

Table 7: RSI calculations—part 2: delta temperature and cumulative temperature (°C) and cumulative heat flux (W/m<sup>2</sup>).

**DATA - January/2017 (Panel EN1A)**

Date Time	Delta temperature				Cumulative $\Delta T$		$\sum_{k=1}^n [\Delta T_k]$		Cumulative Heat Flux (W/m <sup>2</sup> )	
	$\Delta T$ (Stud)	$\Delta T$ (Cavity)	$\Delta T$ (MFP)	$\Delta T$ (Wall)	C_ΔT (Stud)	C_ΔT (Cavity)	C_ΔT (MFP)	C_ΔT (Wall)	HF Stud	HF Cavity
01-0:00	23.37	23.97	6.01	17.96	23.37	23.97	6.01	17.96	11.25	6.52
01-1:00	23.31	24.00	5.85	18.16	46.68	47.98	11.86	36.11	21.93	12.74
01-2:00	23.19	23.91	5.67	18.24	69.88	71.88	17.53	54.35	33.00	18.51
01-3:00	23.04	23.72	5.43	18.29	92.91	95.60	22.96	72.65	43.96	24.44
01-4:00	23.00	23.63	5.34	18.29	115.92	119.24	28.30	90.94	55.87	31.36
01-5:00	23.12	23.76	5.44	18.31	139.03	142.99	33.75	109.25	67.98	37.59
01-6:00	23.13	23.77	5.47	18.30	162.16	166.77	39.22	127.55	80.07	43.72
01-7:00	23.19	23.83	5.49	18.34	185.35	190.60	44.71	145.89	91.60	50.00
01-8:00	23.43	24.08	5.44	18.64	208.78	214.68	50.15	164.53	102.17	55.92
01-9:00	24.17	24.90	5.36	19.54	232.95	239.58	55.51	184.07	116.03	64.60
01-10:00	24.63	25.42	5.10	20.32	257.57	265.00	60.61	204.39	132.60	74.41
01-11:00	24.98	25.81	5.20	20.60	282.55	290.81	65.82	224.99	150.83	84.39
01-12:00	24.68	25.42	4.95	20.47	307.24	316.22	70.77	245.46	165.05	91.82
01-13:00	24.73	25.45	4.97	20.48	331.96	341.68	75.74	265.94	178.53	98.99
01-14:00	25.40	26.12	5.52	20.60	357.36	367.80	81.26	286.55	192.85	107.31
01-15:00	26.26	27.00	6.30	20.71	383.63	394.80	87.55	307.25	207.87	115.01
01-16:00	27.47	28.41	7.71	20.70	411.09	423.22	95.26	327.95	223.16	122.89
01-17:00	28.22	29.47	9.07	20.40	439.31	452.68	104.33	348.35	233.41	127.32
01-18:00	28.95	30.26	9.83	20.44	468.25	482.95	114.16	368.79	242.41	130.87
01-19:00	28.77	29.96	8.85	21.11	497.03	512.90	123.01	389.90	251.54	135.64
01-20:00	28.95	30.22	8.49	21.73	525.98	543.12	131.50	411.62	262.93	142.54
01-21:00	27.96	28.94	7.11	21.82	553.94	572.06	138.61	433.45	272.53	147.27
01-22:00	27.18	28.18	6.22	21.96	581.12	600.25	144.84	455.41	283.31	153.65
01-23:00	27.08	28.21	6.56	21.65	608.20	628.45	151.40	477.06	295.24	159.27
02-1:00	28.85	30.38	8.61	21.76	637.05	658.83	160.01	498.82	307.84	165.73
02-2:00	29.81	31.21	8.81	22.40	666.86	690.05	168.82	521.22	319.73	172.33
02-3:00	30.17	31.70	8.79	22.91	697.04	721.74	177.62	544.13	331.66	178.34
02-4:00	30.79	32.29	8.93	23.36	727.82	754.03	186.55	567.48	344.34	184.86
02-5:00	31.68	33.33	9.47	23.86	759.50	787.36	196.02	591.34	357.18	191.20
02-6:00	32.50	34.22	9.71	24.50	792.00	821.57	205.73	615.84	370.15	198.05
02-7:00	33.25	34.97	10.02	24.96	825.25	856.55	215.75	640.80	382.91	204.68
02-8:00	33.76	35.49	9.92	25.57	859.01	892.04	225.67	666.37	396.86	212.69

The data presented in Table 8 shows the hourly counter, RSI calculated for every hour, and the convergence factor calculation. The RSI was calculated by means of the cumulative temperature divided by the cumulative heat flux at hourly intervals. As recommended by ASHRAE (Flanders, 1985) and ASTM (ASTM, 2013), an interval of between 6 hours and 48 hours can be used as a criteria for the convergence factor to calculate RSI in buildings, depending on the data available. For the convergence factor  $CR_n$ , an interval of  $n=12$  hours was chosen in this study.

Table 8: RSI calculations–part 3: RSI at hourly intervals and convergence factor.

Hour counter	RSI (m <sup>2</sup> *K/ W)				Convergence CRn (n=12)			
	RSI Stud	RSI Cavity	RSI MFP	RSI Wall	Conv Stud	Conv Cavity	Conv MFP	Conv Wall
	1	2.08	3.67	0.92	2.75	0	0	0
2	2.13	3.77	0.93	2.84	0	0	0	0
3	2.12	3.88	0.95	2.94	0	0	0	0
4	2.11	3.91	0.94	2.97	0	0	0	0
5	2.07	3.80	0.90	2.90	0	0	0	0
6	2.05	3.80	0.90	2.91	0	0	0	0
7	2.03	3.81	0.90	2.92	0	0	0	0
8	2.02	3.81	0.89	2.92	0	0	0	0
9	2.04	3.84	0.90	2.94	0	0	0	0
10	2.01	3.71	0.86	2.85	0	0	0	0
11	1.94	3.56	0.81	2.75	0	0	0	0
12	1.87	3.45	0.78	2.67	0	0	0	0
13	1.86	3.44	0.77	2.67	-0.12	-0.07	-0.20	-0.03
14	1.86	3.45	0.77	2.69	-0.14	-0.09	-0.22	-0.06
15	1.85	3.43	0.76	2.67	-0.14	-0.13	-0.25	-0.10
16	1.85	3.43	0.76	2.67	-0.15	-0.14	-0.23	-0.11
17	1.84	3.44	0.78	2.67	-0.13	-0.10	-0.16	-0.09
18	1.88	3.56	0.82	2.74	-0.09	-0.07	-0.10	-0.06
19	1.93	3.69	0.87	2.82	-0.05	-0.03	-0.03	-0.04
20	1.98	3.78	0.91	2.87	-0.02	-0.01	0.01	-0.02
21	2.00	3.81	0.92	2.89	-0.02	-0.01	0.03	-0.02
22	2.03	3.88	0.94	2.94	0.01	0.05	0.09	0.03
23	2.05	3.91	0.94	2.96	0.05	0.09	0.14	0.07
24	2.06	3.95	0.95	3.00	0.09	0.13	0.18	0.11
25	2.07	3.98	0.97	3.01	0.10	0.13	0.20	0.11
26	2.09	4.00	0.98	3.02	0.11	0.14	0.22	0.11
27	2.10	4.05	1.00	3.05	0.12	0.15	0.24	0.12
28	2.11	4.08	1.01	3.07	0.13	0.16	0.25	0.13
29	2.13	4.12	1.03	3.09	0.13	0.16	0.24	0.14
30	2.14	4.15	1.04	3.11	0.12	0.14	0.21	0.12
31	2.16	4.18	1.05	3.13	0.10	0.12	0.17	0.10
32	2.16	4.19	1.06	3.13	0.09	0.10	0.15	0.08
33	2.18	4.22	1.07	3.15	0.08	0.10	0.14	0.08
34	2.18	4.23	1.07	3.16	0.07	0.08	0.12	0.07
35	2.18	4.24	1.06	3.18	0.06	0.08	0.11	0.07
36	2.18	4.22	1.04	3.18	0.05	0.07	0.08	0.06

As mentioned earlier in this section, according to ASTM standard C1155, a convergence factor of  $CV_n < 10\%$  is required for at least three periods of length  $n$ . The valid RSI and corresponding R-value results were then combined and summarized as presented in Table 9. These results are from the period of January 1–15, 2017 for panel EN1A (Edmonton, north, position 1, “Type A”).

Table 9: RSI calculation results: summary of results for panel EN1A from January 1–15, 2017.

Calculation–EN1A–Jan 1–15, 2017						
	Hour	Conv. Stud	Conv. Cavity	Conv. MFP	Conv. Wall	Conv. Total Assembly
RSI (m <sup>2</sup> .K/W)						
Trial 1	108	1.953531	3.949419	0.850924	3.098495	3.550242
Trial 2	145	1.99524	4.036441	0.897836	3.138605	3.628201
Trial 3	182	2.006207	4.046597	0.899639	3.146959	3.638519
Trial 4	219	2.021159	4.070315	0.906711	3.163603	3.660483
Trial 5	256	2.013117	4.066082	0.899302	3.16678	3.655489
Trial 6	293	2.013647	4.069558	0.888719	3.180839	3.658376
Trial 7	330	1.998422	4.036668	0.877023	3.159645	3.629019
Trial 8						
Average		2.000189	4.039297	0.888593	3.150704	3.631476
St. Dev.		0.022468	0.042312	0.019163	0.026768	0.038312
COV%		1.123%	1.047%	2.157%	0.850%	1.055%
Summary of Results						
		Stud	Cavity	MFP	Wall	Total Assembly
RSI	m <sup>2</sup> *K/W	2.000189	4.039297	0.888593	3.150704	3.631476
R-value	F*ft <sup>2</sup> /Btu	11.35759	22.93618	5.045664	17.89052	20.62046

Table 6 through Table 9 demonstrate the first 36 hours of calculations for the panel EN1A (Edmonton, north, position 1, “Type A”) from the period of January 1–15, 2017. The calculations above represent a three-day sample, while this procedure was applied for all panels for a period of over two years in both locations, the results of which will be discussed in the following sections.

## 4.2 Indoor Temperature Distribution on Tested MFPs

Another important aspect to be investigated in a hygrothermal performance evaluation of building envelope is the temperature distribution. The heat transfer in a building envelope, which is a natural phenomenon that happens by the difference between indoor and outdoor temperature, can impact in the indoor temperature distribution. The heat flows from the side of higher temperature to the side with lower temperatures. It should be noted that higher variations on the indoor temperature distribution can impact the wall system functionality.

In this study, temperature sensors were installed at three vertical levels to measure the performance of the tested MFPs in terms of the uniformity of the indoor temperature gradient distribution. The evaluation results are demonstrated by comparing the performance of “Type A” and “Type B” wall assemblies along with the “Type C” wall assembly, which represents the conventional wall system practice. Sensors T3, T8, and T13 were attached to the interior layer of the MFPs at the upper, middle, and lower vertical levels. The data used to analyze the temperature distribution was collected between August 2015 and March 2018.

For each panel, the minimum, maximum, and average differential temperatures between the three sensors were calculated as summarized in Table 10. Panel EN1A, located at the western edge of the wall, achieved the maximum difference of 2.30°C with an average of 0.52°C. On the other hand, panel EN4A, which is identical in its components to EN1A but is located in the middle of the wall rather than at the wall’s edge, measured a significantly lower differential temperature, with a maximum of 1.60°C and an average of 0.24°C.

The “Type B” panels demonstrated a comparable measurement between EN2B and EN5B, having a maximum of 2.31°C and 2.29°C and an average of 0.47°C and 0.39°C, respectively. By comparing the wall assemblies with the MFPs attached to their exterior surfaces with the

conventional wall assembly, which does not include any of the MFPs (i.e., EN3C), it was found that the MFPs play a vital role in conveying the uniform distribution of temperature within the interior layers of their corresponding wall assemblies. For example, for EN3C, the variation of the differential temperature between the outdoor and indoor surface temperatures among the three vertical levels is significantly higher when compared to the other wall assemblies that have MFPs attached to them within the same location and wall orientation as summarized in Table 10.

It was found that the variation in the differential temperatures at the three vertical levels of each wall assembly is directly dependent on the type of MFP attached to the conventional wall assembly. For example, it can be observed that the “Type A” MFP (i.e., wood fibre) has the least variation in temperature distribution, in other words, maximum temperature uniformity within the height of the wall, followed by the “Type B” MFP (i.e., XPS), and finally the “Type C” MFP, which reveals the highest temperature variation.

For the south positioned panels, where solar radiation contributes to a significant impact on the vertical temperature distribution within each wall assembly, it can be observed that the MFPs can thus improve the uniformity of the interior surface temperatures of the wall assemblies attached to them. The “Type A” east-positioned panels, ES1A and ES4A, measured maximum differences of 10.61°C and 6.39°C with an average of 0.56°C and 0.57°C. Even with higher maximum variation the average of differences is comparable with north-positioned panels.

For “Type B” panels, ES2B and ES5B, the maximum difference in temperature reached 11.60°C and 6.97°C with an average of 0.65°C and 0.72°C. Upon comparing “Type A” panels with “Type B” panels, notably, on average, “Type A” panels exhibit a better performance. For the assembly with no panel attached, the maximum difference achieved was 17.58°C with an average of 0.77°C. These measurements are much higher than those for the panels with the MFP attachment.

The maximum measurements for “Type A” panels reached 7.46°C and 5.09°C with an average of 0.38°C and 0.59°C. For “Type B” panels the maximum measurements were 6.48°C and 5.40°C with averages of 0.52°C and 0.51°C. When comparing the “Type A” and “Type B” wall assemblies to the “Type C” wall assembly with no MPF attached, the higher maximum differential temperature of 14.88°C and average of 0.66°C can be observed.

Consequently, it can be concluded that the attachment of the MFPs to the exterior side of the conventional wall assemblies can potentially contribute to the improvement of the thermal performance of these wall assemblies in terms of the uniform distribution of indoor wall surface temperatures regardless of the wall orientation (i.e., north, south) or location (i.e., Edmonton, Vancouver). However, in some cases, such as for those panels positioned at the south in the Edmonton test hut, the “Type A” MFP has shown a slightly better performance than that of “Type B”.

Table 10: Vertical variation in temperature distribution in Edmonton and Vancouver.

Edmonton North Facing Panels					
°C	EN1A	EN2B	EN3C	EN4A	EN5B
Min	0.007	0.007	0.008	0.001	0.004
Max	2.30	2.31	3.91	1.60	2.29
Avg	0.53	0.47	0.58	0.24	0.40
Vancouver North Facing Panels					
°C	VN1A	VN2B	VN3C	VN4A	VN5B
Min	0.012	0.003	0.002	0.004	0.011
Max	2.06	2.68	2.78	2.20	2.57
Avg	0.42	0.34	0.51	0.49	0.39
Edmonton South Facing Panels					
°C	ES1A	ES2B	ES3C	ES4A	ES5B
Min	0.005	0.001	0.002	0.002	0.007
Max	10.61	11.61	17.59	6.34	6.98
Avg	0.56	0.65	0.78	0.58	0.71
Vancouver South Facing Panels					
°C	VS1A	VS2B	VS3C	VS4A	VS5B
Min	0.001	0.002	0.002	0.003	0.002
Max	7.47	6.49	14.89	5.10	5.40
Avg	0.39	0.53	0.67	0.60	0.51

It was noted that in both locations, the wall assemblies with the attachment of either “Type A” or “Type B” MFPs on the exterior surface contributed to the vertical indoor temperature distribution. It was also observed that the south-oriented walls demonstrated a higher variation in temperature distribution than north-oriented walls. This phenomenon was expected due to the impact of solar radiation; furthermore, at the upper levels of the wall assemblies the variation was higher than at the lower levels.

The improvement of the interior temperature distribution can also be seen when comparing the results from temperature measurements for the three wall assemblies analyzed in this study for one day in both locations (Edmonton and Vancouver) and wall orientations (North and South). The

“Type A” is represented in green, “Type B” in pink and “Type C” in yellow as represented in Figure 18.

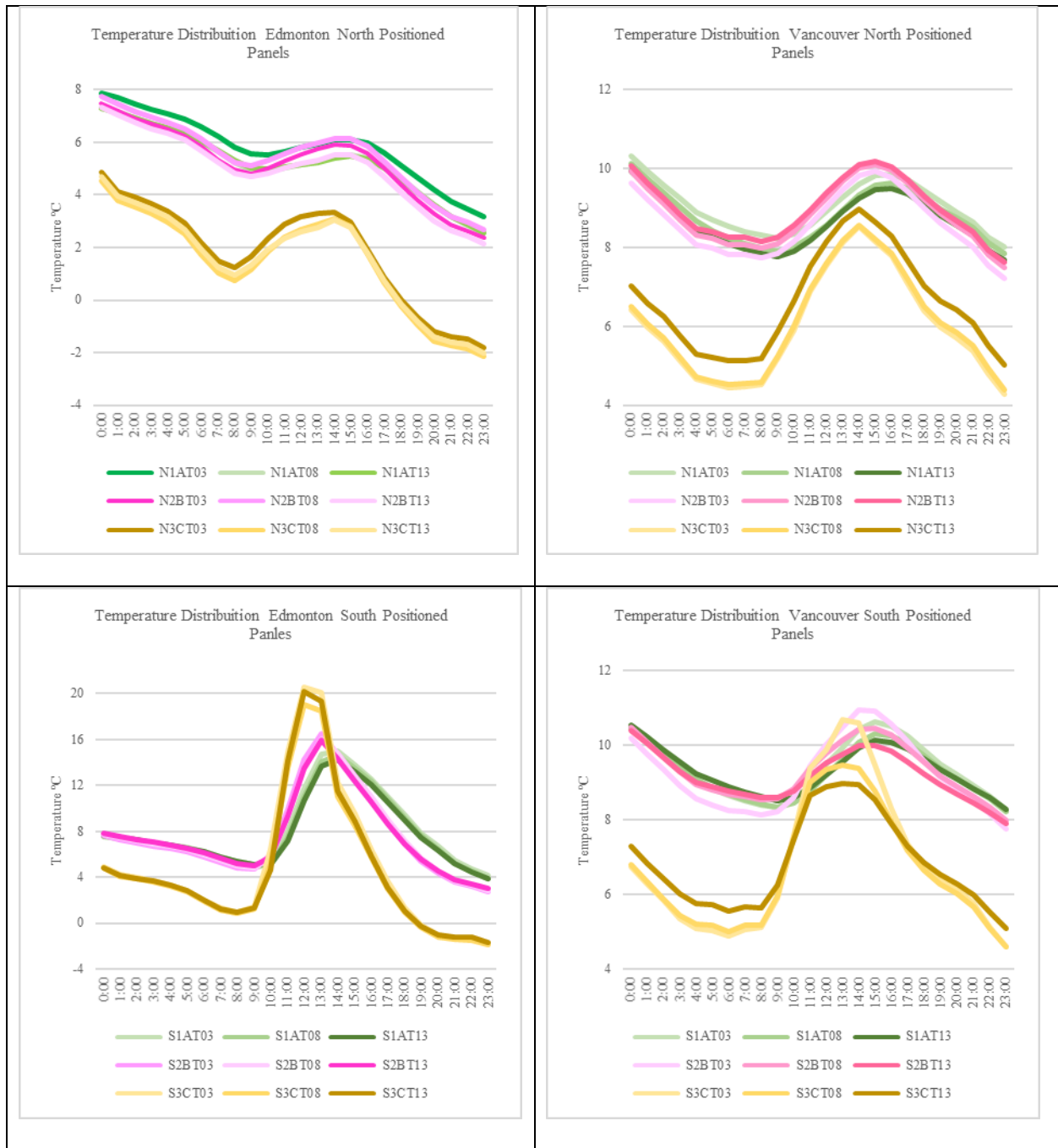


Figure 18: Temperature distribution profiles, north and south positioned panels, Edmonton, and Vancouver.

A summary of the average vertical variation in temperature distribution along the three vertical levels of inner wall assembly layers, sensors T03, T08, and T13, for both locations at north and south orientations are presented in Figure 19. Notably, the performance for both “Type A” and “Type B” panels for the north Edmonton location is similar.

On the other hand, the south Edmonton location “Type A” panel performs slightly better than “Type B”. It is important to note, however, that in Vancouver both “Type A” and “Type B” panels have a similar performance in the south location, but the north location “Type B” performs better than “Type A”. One possible explanation is that the high humidity levels in Vancouver’s climate contribute to the better performance of “Type B” than “Type A” in the north orientation where there is no direct solar radiation impact.

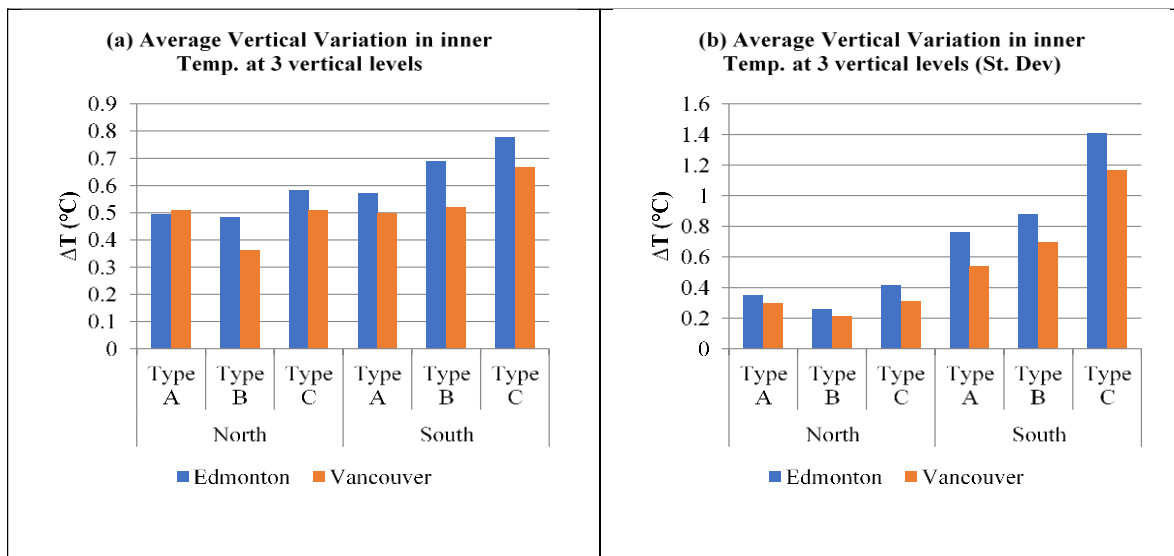


Figure 19: Average variation of temperature distribution on three vertical levels of the inner wall assembly.

### 4.3 Impact of Thermal Bridge and Thermal Mass Performance

Thermal bridging takes place when any conductive element bypasses the insulation, allowing more heat to flow, resulting in raising or reducing the interior temperature. The impact of thermal bridging was investigated in this thesis; the results from the heat flux sensors placed on the interior surface of the MFPs at both the cavity and stud locations were compared to the conventional wall assembly and no clear difference was found at either location (Edmonton and Vancouver). On the other hand, when analyzing temperature profiles, it can be observed that wall assembly “Type C” allows the heat (gain/loss) to pass through the wall more quickly than the wall assemblies with the MFPs attached to the exterior side, which indicates a lower thermal performance and higher thermal bridge. Data from the temperature profiles from the middle vertical layer is combined with interior and exterior temperature profiles as follows:

- T\_amb: indoor ambient temperature;
- T10: indoor surface temperature;
- T\_ins: temperature inside the insulation cavity;
- T08: temperature on interior surface of MFP;
- T07: exterior surface temperature; and
- T\_out: outdoor temperature.

The average temperature values within each layer in correspondence to outdoor temperature were grouped by increments of 10°C in order to visualize the differential temperature between outer and inner layers as presented in

It can be observed that the wall assemblies with the highest thermal resistance reveal the highest differential temperature between the internal and external surfaces of the wall, especially in extreme weather conditions. It can also be observed that, in the “Type C” wall assembly, with no MFP attachment, the measurement from sensor T08 (temperature at the outer surface of the conventional insulation surface and the inner surface of the MFP) and sensor T07 (outdoor surface temperature) are approximately equal. On the other hand, the “Type A” wall assembly demonstrated a slightly better performance than the “Type B” wall assembly in terms of resistance to thermal bridging. The measurements from temperature sensors T07, T08, T10, T\_ins, and T\_amb were collected for the 20 panels in both locations as presented in Figure 20.

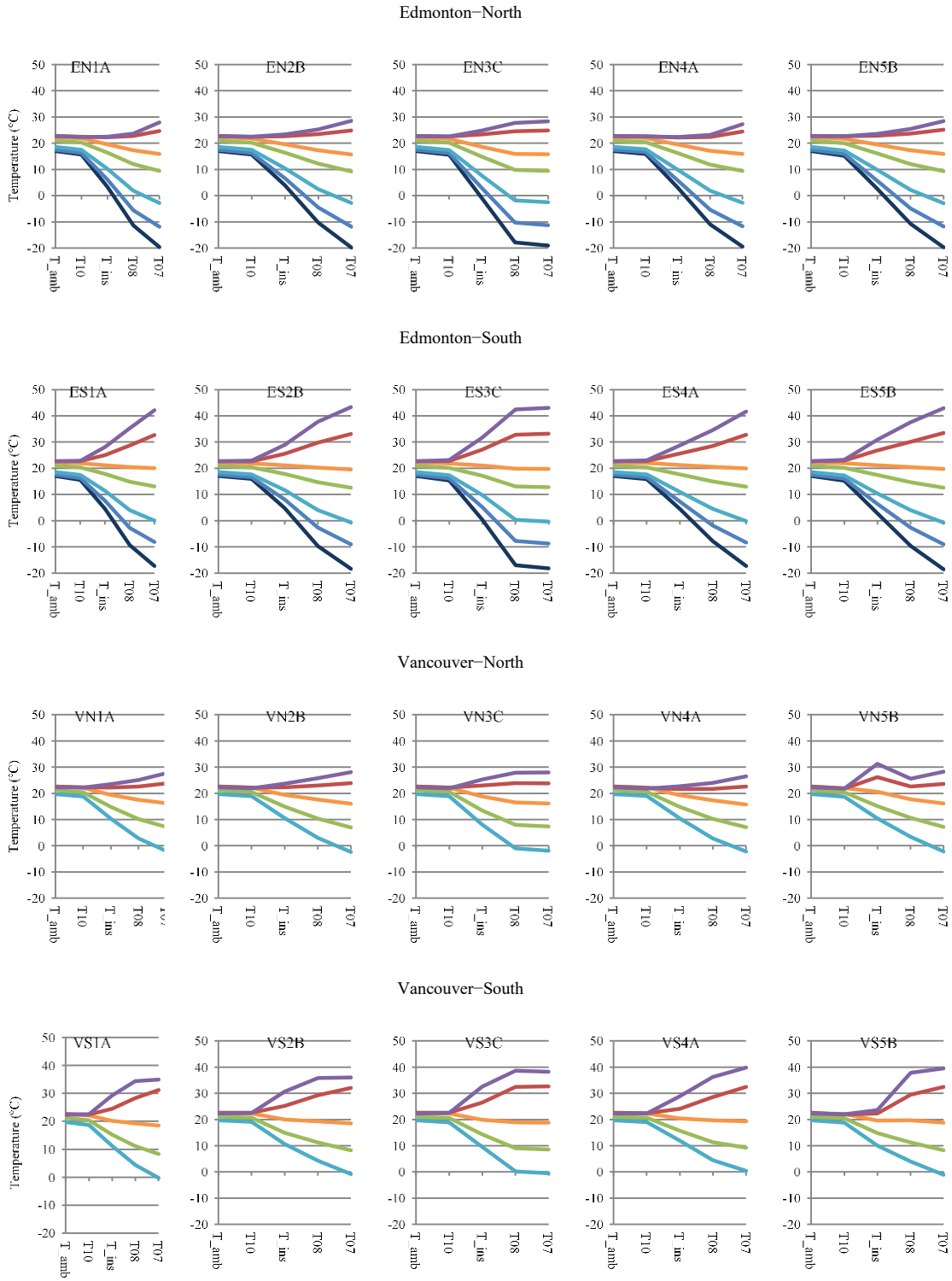


Figure 20: Temperature in various wall layers in Vancouver and Edmonton for three different wall assemblies.

Another important aspect of material performance in building envelope systems is the capacity to store heat. The capacity of heat storage of a material is called thermal mass. Materials with high thermal mass absorb thermal energy from the sun, conduct a significant portion into the material, and it is released over time. Depending on the climatic conditions, optimal thermal mass (which is a combination of density and specific heat capacity) can potentially reduce the annual energy (heating and cooling) consumption of a building (ASHRAE, 1991). When comparing to other materials used in insulation, wood fibre has a much higher density and its heat capacity achieves  $2.3 \text{ J}/(\text{g}\cdot\text{K})$ .

The thermal mass of the MFPs was assessed in this research and the evaluation was conducted by comparing the temperature gradients provided by the thermocouples attached to the interior side of the MFPs. The data was analyzed and hourly temperature results from the different wall assemblies were compared. As presented in Figure 21, the temperature measurements from sensor T08 (positioned on the interior layer of the MFPs) were combined hourly for the month of January to facilitate the visualization of the thermal mass effect. It can be observed that the MFP “Type A” released heat absorbed by the sun more slowly than MFP “Type B” followed by the “Type C” wall assembly for both locations (Edmonton and Vancouver) and orientations (north and south). When comparing north-facing with south-facing wall assemblies, the difference is even more visible.

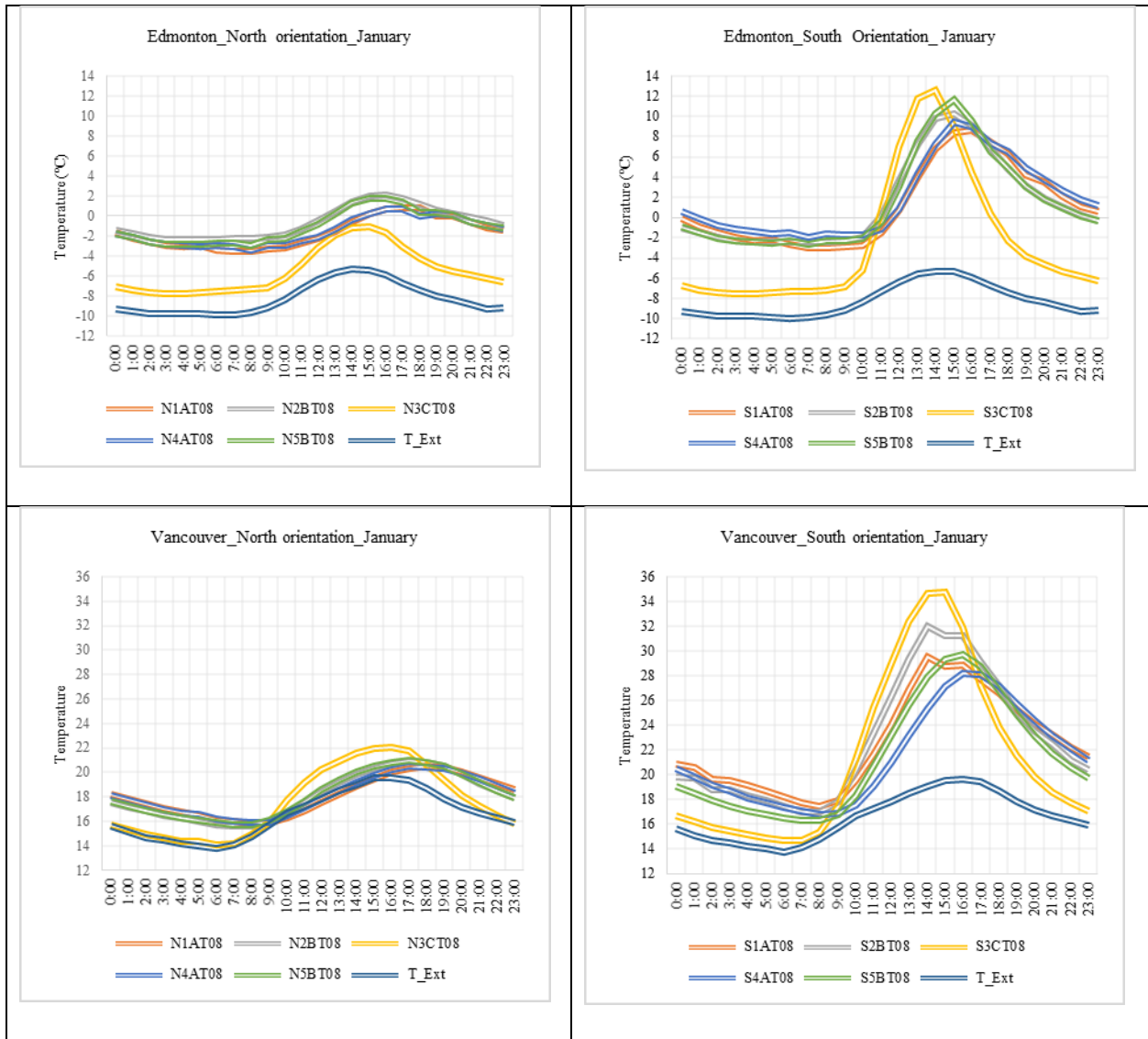


Figure 21: Hourly temperature profile in the interior layer of the MFPs for Edmonton and Vancouver locations.

#### 4.4 Moisture Content Levels in the MFPs

Moisture accumulation inside the building envelope can cause mold and thus lower the overall hygro-thermal performance of a building. An incorrect design and material selection can adversely affect the long-term moisture performance of the building envelope (Salonvaara, M., Karagiozis, A., Holm, A., 2001). Moreover, when the material’s moisture storage capacity is exceeded, decay and proliferation of mold can occur.

For this reason, the moisture content in the proposed MFPs is analyzed in this section over different climatic conditions. In order to analyze the impact of moisture on the material's performance, moisture content sensors were placed at three vertical levels and on the outer layer (M01, M04, and M07) and inner layer (M02, M05, and M08) of each panel.

To begin the analysis, the moisture content (MC) levels at the inner layer of the "Type A" MFP located in Vancouver for both north and south orientations are presented in Figure 22. The MC levels range between a minimum of 8.65% at VS4A (south-east) and maximum of 12.97% at VN4A (north-east), respectively. As expected, panels facing south show a higher variation on moisture content levels because of the impact of solar radiation. Therefore, on the outer layer of "Type A" panels in Vancouver, the variation in moisture content levels is higher on north positioned panels than in south positioned panels. For the "Type A" south-facing panels (VS1A and VS4A), moisture content levels vary from 7.82% to 12.81% and for the north-facing panels (VN1A and VN4A) of the same material, the moisture content levels range from 9.71% to a maximum of 18.14%. Higher moisture content levels were expected for Vancouver because of the impact of the humid climate conditions on the panels. North-facing panels tend to dry out at a slower pace and consequently accumulate higher levels of moisture.

On the other hand, for the inner layer of the "Type B" panels of the Vancouver test hut, the maximum MC was measured by the sensor applied at the north-west position (VN2B) and achieved 13.25%, and the minimum percentage of MC was 8.61% and was measured for the panel ES5B (south-east). For the outer layer, the maximum MC level was measured for the north-west positioned panel (VN2B) and achieved 18.63%, and the minimum MC level of 7.60% was measured for the south-west positioned panel (VS2B). By comparing the MC levels for the outer

and inner layers of the same wall system, it was found that the fluctuations in the MC levels are higher for the outer layers than those for the inner layers, as presented in Figure 22.

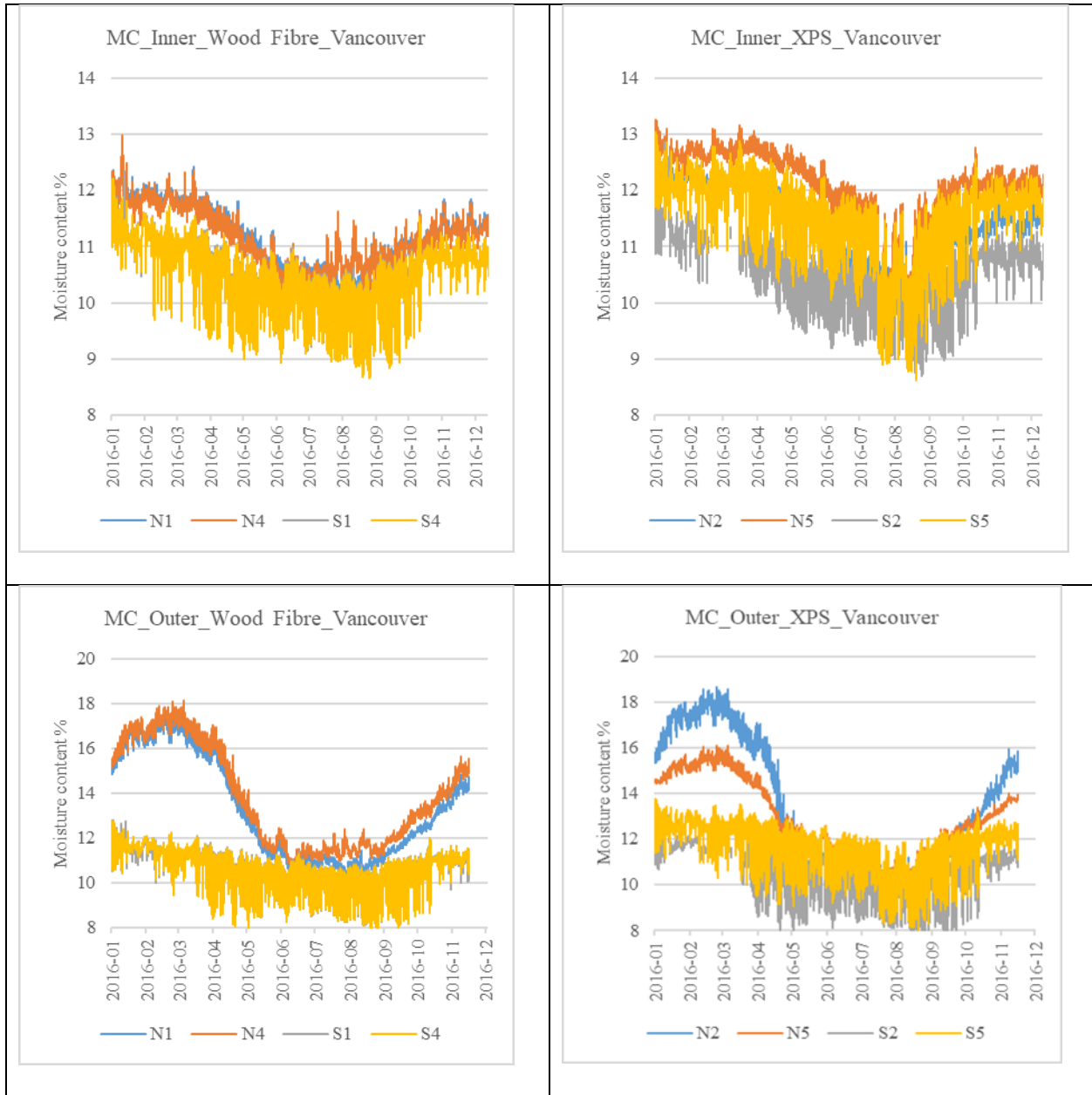
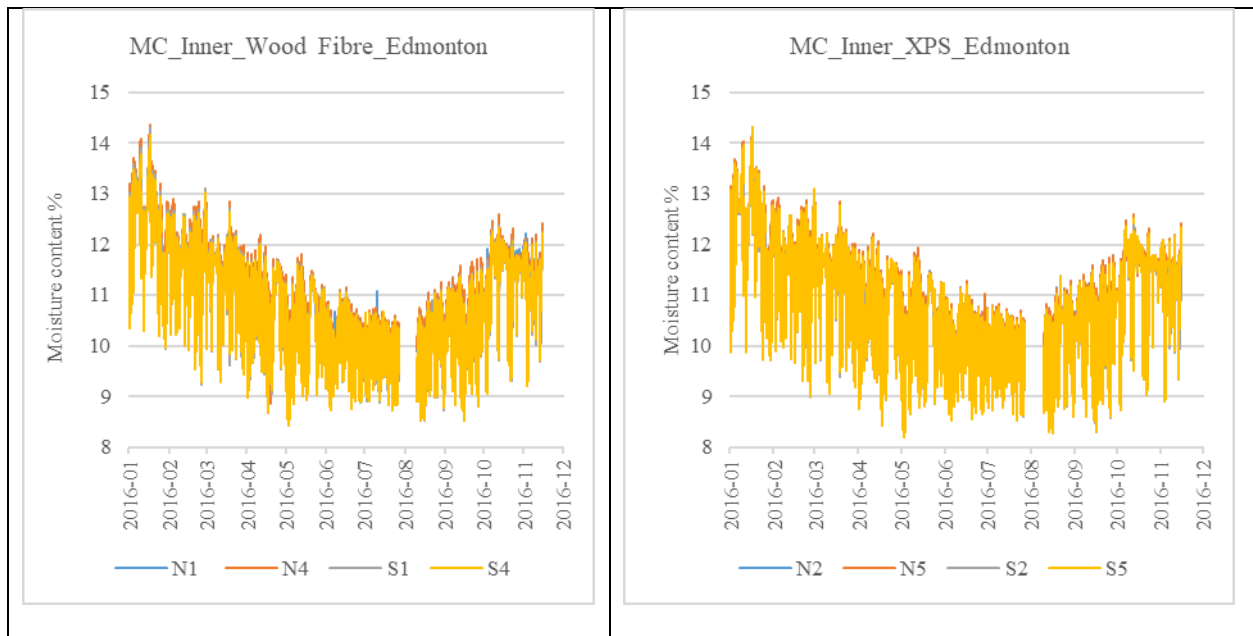


Figure 22: Moisture content levels for inner and outer layers of MFPs in Vancouver location.

The following graphs present the results for the Edmonton location. Figure 23 demonstrates measurements from the inner and outer layers, “Type A” and “Type B”, north and south panels.

By analyzing the results from the inner layer of “Type A” panels, it was found that the maximum percentage of MC was measured by the sensor applied on panel EN4A (north-east) and achieved 14.35%, and the minimum measurement was from sensor ES4A (south-east) and was as low as 8.42%. For the outer layer of “Type A”, the maximum percentage of MC measured 15.54% for panel EN1A, a north-west positioned panel with a lower amount of solar radiation, and the minimum measurement of 7.61% was found on panel ES4A, a south-east positioned panel with the direct impact of solar radiation to stimulate the drying of the material.

Additionally, the MC of the “Type B” panels applied to the inner layer of the Edmonton test hut were also measured and it was found that the maximum MC levels of EN2B (north-west) panel of was 14.30% and the minimum was 8.19% on the south-east positioned panel (ES5B). The higher MC measurements were collected in the winter period and, conversely, the lower measurements were collected during warmer months. The MC for the outer layer of “Type B” panels presented a maximum measurement at panel EN2B (15.59%) and the minimum at panel ES5B (7.38%) as presented in Figure 23.



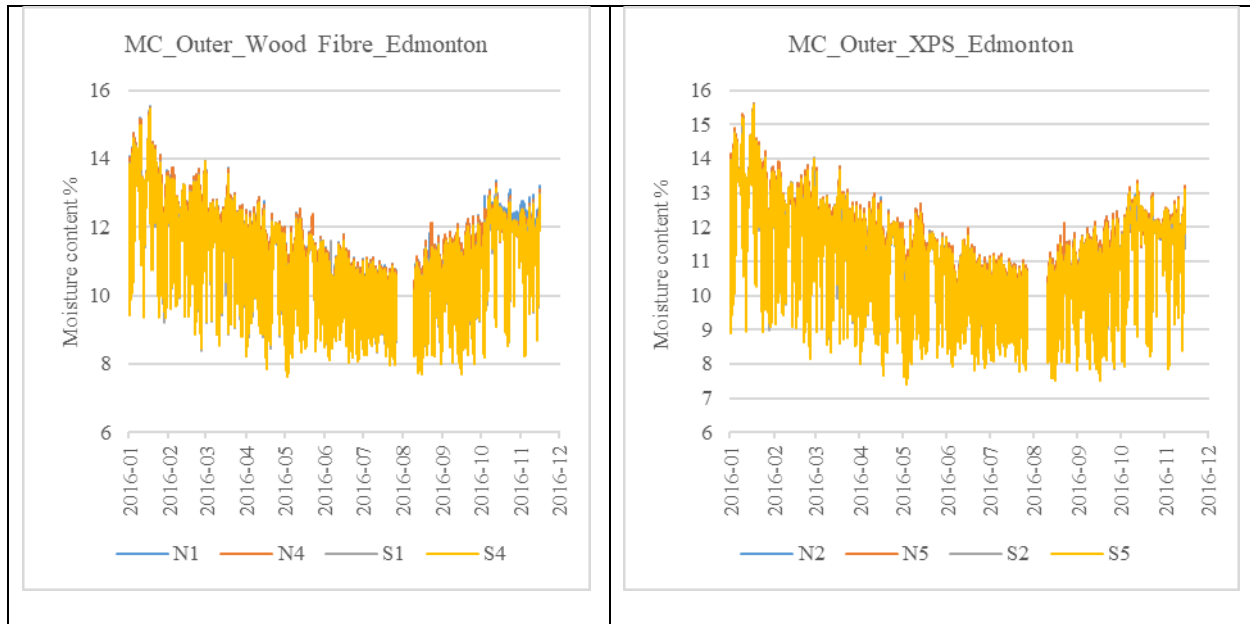


Figure 23 : Moisture content levels for inner and outer layer of MFPs in Edmonton location.

#### 4.5 Vapour Control in the Insulation Panels

As mentioned in the previous section, in order to achieve an energy-efficient design, knowledge of how materials handle moisture is necessary. Excess moisture can lead to proliferation of mold and thus decrease the building envelope’s hygro-thermal performance. Therefore, vapour transmission plays an important role on the overall assembly’s moisture behaviour as lack of proper vapour diffusion control strategy can adversely impact both the short- and long-term hygrothermal performance.

It is important to note, however, that vapour diffusion affects the building envelope’s performance in many ways, depending on the climatic conditions and interior conditions of the building throughout the year (Lstiburek, 2002). Moreover, the use of a vapour barrier can help to control moisture movement through the wall assembly (Mu, khopadhyaya, Ping, Kumaran, & Van Reenen, 2009). In order to analyze the vapour control in the wall systems, relative humidity and

temperature sensors were placed at different locations of the walls to evaluate how the MFPs manage various levels of humidity.

An analysis of measurements from the relative humidity sensors and temperature sensors placed on the interior layer of the wall was conducted and is presented in Figure 24. Results from these sensors show higher relative humidity rates and lower temperature profiles for the “Type C” wall assembly as no MFP is attached to minimize the impact of weather conditions. Panel EN4A placed in a north-west position measured a slightly higher relative humidity than panel EN1A positioned at north-east. The temperature profiles of “Type B” wall assemblies are similar to those of “Type A” wall assemblies. On the other hand, the relative humidity is higher in “Type B” than that of “Type A”, even higher than that of “Type C” wall assembly in some periods. In this context, this physical characteristic of “Type B” MFPs is deemed to increase the possibility of the proliferation of mold. In south-facing panels, with the impact of solar radiation, the temperature and relative humidity variations are higher than for those in the north-facing panels. For the relative humidity levels of south-oriented “Type A” panels, by comparing “Type A” south-facing panels with the “Type C” conventional wall assembly, it can be observed that the higher variations in temperature and relative humidity were measured in the conventional wall assembly, followed by the south-west positioned panel (ES4A), and finally the south-east panel (ES1A). The relative humidity levels for panel ES2B and ES5B are higher in some periods than the conventional wall and the temperature profiles present higher variation than north-facing panels.

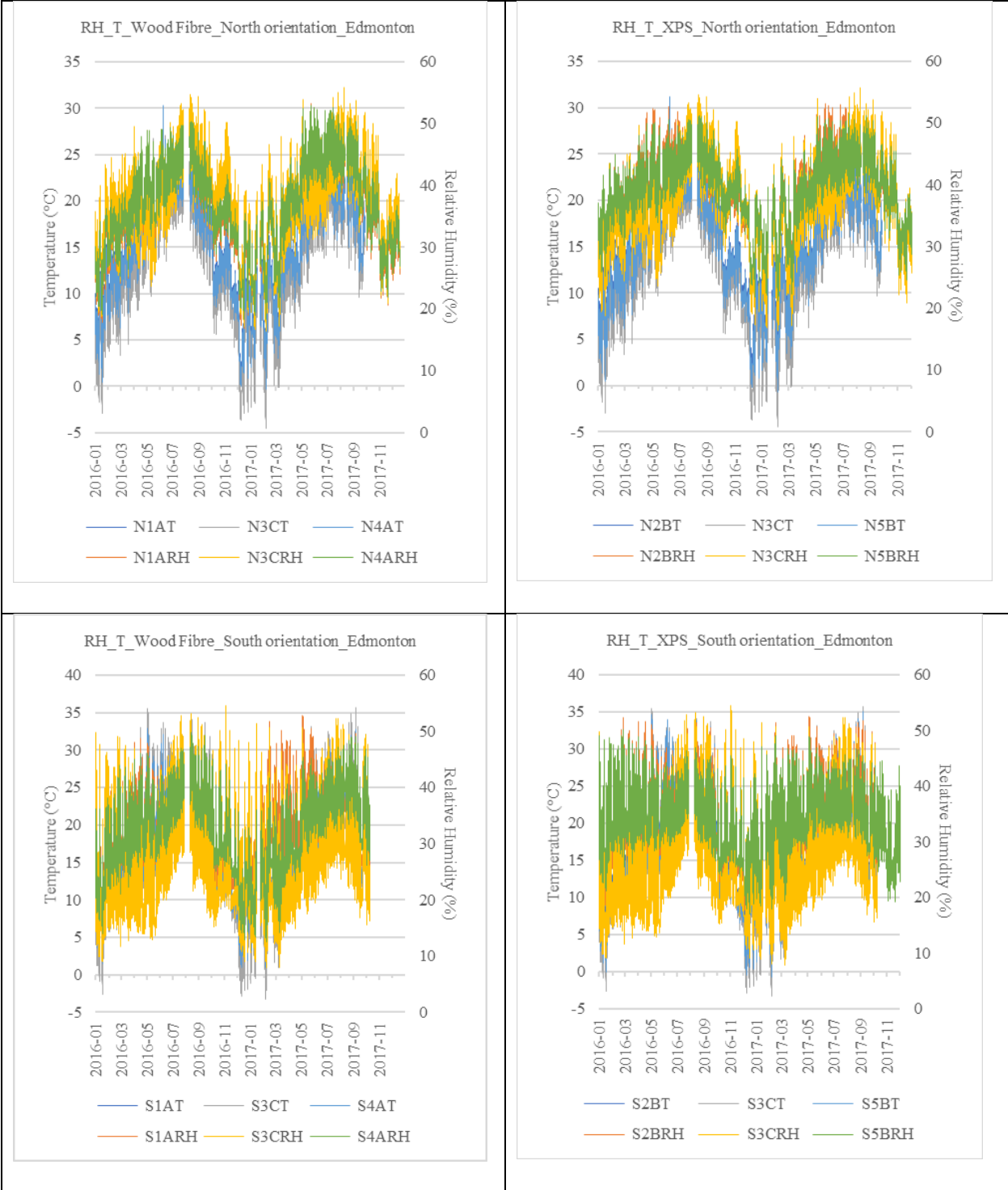
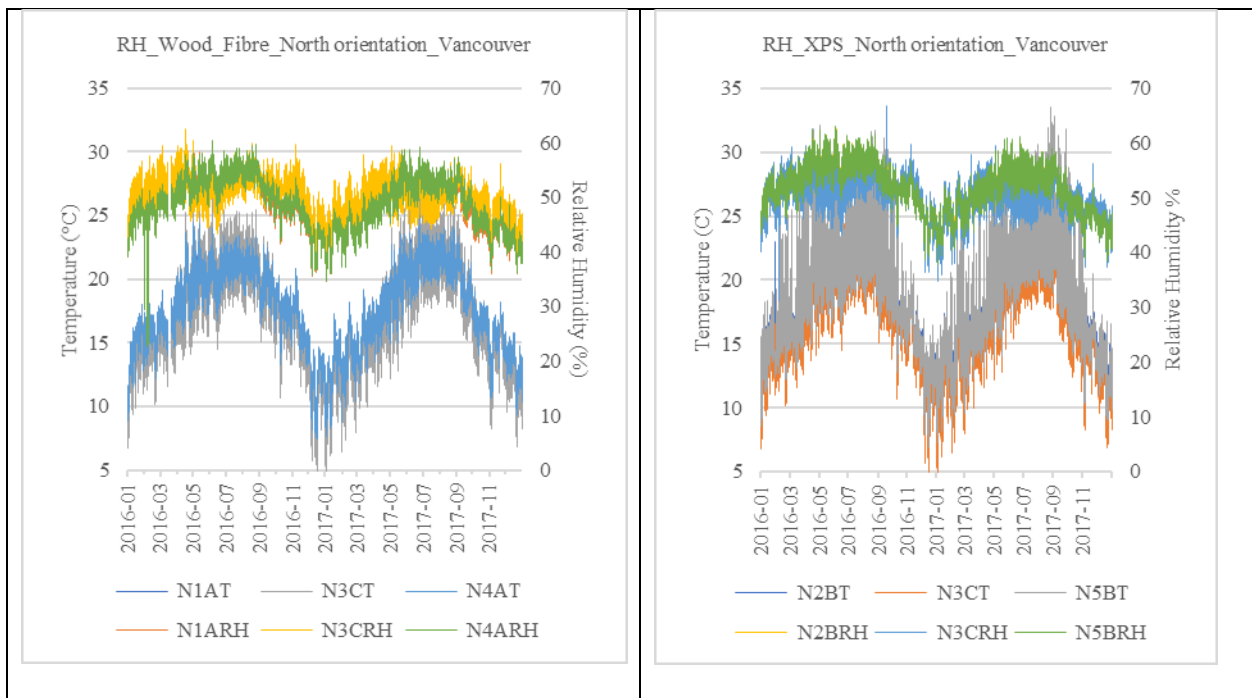


Figure 24: Relative humidity and temperature profiles in North and South facing wall assemblies in Edmonton location.

The impact of the climate conditions can be observed in Vancouver when compared to Edmonton in terms of the Relative Humidity measurements as presented in Figure 25. Edmonton shows significantly lower levels of Relative Humidity than Vancouver; however, the MFP performance presents some similarities. Similar to Edmonton, results from the Vancouver “Type C” wall assembly show higher relative humidity rates and lower temperature profiles as no MFP is attached to minimize the impact of weather conditions.

As observed for most of the measurements from north-positioned panels, VN1A and VN4A show slightly lower relative humidity levels than panels VN2B and VN5B, which indicates that MFP “Type A” allowed moisture to escape at a faster rate than MFP “Type B”. In the south-positioned panels, where solar radiation could impact the levels of relative humidity, the MFP “Type A” still present lower measurements than MFP “Type B”, and “Type C” (with no attachment of MFP) has the highest relative humidity levels.



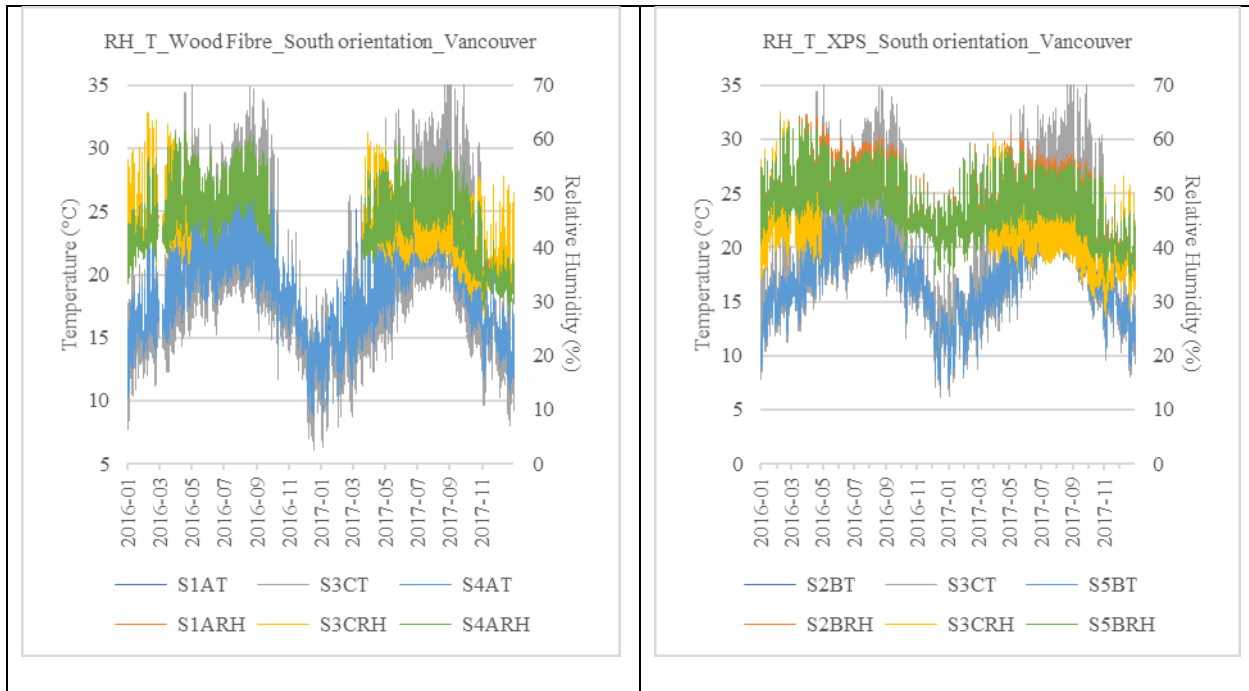


Figure 25: Relative humidity and temperature profiles, North and South facing wall assemblies in Vancouver location.

#### 4.6 Discussion of Hygrothermal Performance

In this section, results from the long-term hygrothermal field testing performance of the MFPs will be discussed. As presented in the previous sections, an incorrect design can affect the overall hygrothermal performance of a building. A combination of various parameters should be analysed in order to provide a complete hygrothermal performance evaluation. In this research correlated parameters such as the thermal resistance, thermal bridging, thermal mass performance, temperature distribution, moisture content levels, humidity levels and weather conditions were investigated for all wall systems. The performance of a building envelope is affected by a combination of factors like air leakage, moisture infiltration and heat movement. Thermal resistance is determined by heat flux and temperature measurements, thermal bridging is directly related to air leakage, thermal mass is the capacity of the material to store heat and release it over time and, the capacity of materials to handle moisture directly impact the overall performance as well as the indoor and

outdoor conditions. For this reason, real-time measurements of moisture content, temperature, and indoor and outdoor environmental conditions were used to determine the hygrothermal performance of the wall systems.

To begin, the thermal performance measurement results are presented in this section. The RSI calculations were carried out between August 2015 and February 2018 in both locations, Edmonton and Vancouver. Temperature sensors (T6, T7, T8, T9, and T10) and heat flux sensors (F1 and F2) were used for the RSI calculations. As explained in section 4.1, the RSI values were calculated according to the ASTM standard and the physical proportions of the stud and cavity were considered in the tested wall per unit area.

According to the ASTM standard, the coefficient of variation (COV) should not exceed 10%. It is important to note, however, that in the calculations of the present study, some of the results did not meet this criterion due some possible malfunctioning of sensors, specifically heat flux sensors, which often consume more battery power compared to other sensors involved in this study. To check measurements results from some heat flux sensors, XPS material was chosen due the stability of the material. The theoretical calculation was made using steady state formulas from Fourier's law. First, the calculation of heat flow was made using the Eq. 4:

$$Q = A * \frac{k}{l} * (\Delta T) \quad (5)$$

Where  $Q$  is the rate of heat flow,  $A$  is the area,  $K$  is the thermal conductivity,  $l$  is the length of the flow path or thickness of material and  $\Delta T$  is the temperature difference producing the flow. The heat flux is the heat flow per unit of area as described in the Eq. 5:

$$q = \frac{Q}{A} \quad (6)$$

Where  $q$  is the heat flux,  $Q$  is the rate of heat flow and  $A$  is the area. The equations describe steady-state flow in one direction along the cross section of the path. The coefficient  $K$  is the rate of steady state heat flow through a unit area of a uniform material induced by a unit of temperature difference. The technical bulletin from the extruded polystyrene rigid foam insulation (XPS) by Owens Corning Formular used in this project provides the thermal conductivity coefficient of  $0.029 \text{ W/m}\cdot\text{K}$ . A sample of data from the panel ES2B (Edmonton, south orientation, position 2, MFP “Type B”) was selected and the theoretical heat fluxes were then calculated as demonstrated in Table 11.

Table 11: Comparison between heat flux measured data and calculated heat flux.

DateTime	Temperature °C			Heat flux W/m <sup>2</sup>	
	S2BT07	S2BT08	ΔT	Calculated	Measured
2016-01-01 0:00	-8.12	-0.17	7.95	9.23	0.38
2016-01-01 1:00	-8.28	-1.07	7.21	8.36	3.14
2016-01-01 2:00	-8.47	-1.62	6.84	7.94	2.68
2016-01-01 3:00	-9.36	-2.12	7.24	8.40	5.74
2016-01-01 4:00	-9.35	-2.53	6.82	7.91	7.17
2016-01-01 5:00	-9.04	-2.59	6.45	7.49	5.01
2016-01-01 6:00	-9.72	-2.67	7.05	8.17	4.75
2016-01-01 7:00	-10.53	-3.01	7.53	8.73	5.40
2016-01-01 8:00	-10.59	-3.43	7.15	8.29	2.24
2016-01-01 9:00	-9.61	-3.64	5.98	6.93	1.47
2016-01-01 10:00	-1.98	-2.96	-0.97	-1.13	2.05
2016-01-01 11:00	16.24	2.15	-14.08	-16.34	3.70
2016-01-01 12:00	25.88	10.26	-15.62	-18.12	1.23
2016-01-01 13:00	29.60	17.00	-12.61	-14.62	4.24
2016-01-01 14:00	20.74	20.43	-0.31	-0.36	3.42
2016-01-01 15:00	9.10	18.26	9.16	10.62	1.96
2016-01-01 16:00	3.71	14.49	10.78	12.50	-0.93
2016-01-01 17:00	-0.38	10.64	11.02	12.79	1.49
2016-01-01 18:00	-2.83	7.60	10.43	12.09	2.29
2016-01-01 19:00	-4.17	5.16	9.32	10.82	1.52
2016-01-01 20:00	-4.70	3.55	8.25	9.57	2.95
2016-01-01 21:00	-4.84	2.60	7.44	8.63	3.60
2016-01-01 22:00	-5.76	1.86	7.63	8.85	1.39
2016-01-01 23:00	-6.07	0.99	7.06	8.19	0.69
2016-01-02 0:00	-6.44	0.36	6.81	7.89	1.18
2016-01-02 1:00	-7.01	-0.20	6.81	7.90	2.88
2016-01-02 2:00	-7.97	-0.82	7.15	8.29	3.11
2016-01-02 3:00	-8.63	-1.52	7.11	8.25	2.21
2016-01-02 4:00	-9.03	-2.10	6.93	8.04	3.91
2016-01-02 5:00	-9.24	-2.50	6.74	7.82	7.10
2016-01-02 6:00	-9.26	-2.66	6.60	7.65	7.23
2016-01-02 7:00	-9.54	-2.75	6.79	7.87	4.04
2016-01-02 8:00	-9.50	-2.86	6.64	7.71	4.86
2016-01-02 9:00	-8.82	-2.83	5.99	6.95	3.58
2016-01-02 10:00	-4.00	-2.43	1.57	1.82	1.59
2016-01-02 11:00	13.12	1.82	-11.30	-13.11	1.31
2016-01-02 12:00	22.07	8.84	-13.23	-15.35	2.75
2016-01-02 13:00	25.89	14.87	-11.02	-12.78	4.86
2016-01-02 14:00	18.15	18.24	0.08	0.10	3.45
2016-01-02 15:00	6.70	16.48	9.78	11.34	0.38

When comparing the calculated results with the measured data, it was noticeable that some malfunctioning on the sensors measurements occur and in this regard, the wall assemblies with malfunctioning sensors were not considered for RSI calculations. In this case, in the average calculations, panel “Type A” Vancouver, north orientation and Edmonton “Type B”, south orientation were desconsidered in the final analyses.

The proposed MFPs, “Type A” and “Type B”, were designed to add an R-value of 5 F\*ft<sup>2</sup>/Btu or an RSI of 0.88 m<sup>2</sup>\*K/W to the wall assemblies. When compared with the calculated results from the field data, it was observed that most of the RSI values calculated are comparable to the expected results from the material itself, with the exception of the “Type A”, Vancouver, north panel, “Type B” Vancouver south panel and “Type B”, Edmonton, south panel. In these cases, the results were higher than those of their respective locations. This variability can be related to a number of technical issues such as construction quality, sensors accuracy, impact of solar radiation on the thermal performance of the tested walls, or overseen causes. Also in the “Type C”, Vancouver, south wall assembly the results were not considered in the final analyses as the results were again higher than expected for the constructed wall assembly.

To understand another perspective of the thermal performance, an analysis of the temperature profiles was conducted for all the panels with MFPs attached to their exterior side. The temperature measured by the weather station was then compared to the results provided by the sensor T08 installed on the interior surface of the MFP. Results from temperature variations from Vancouver and Edmonton, north and south orientations, are presented in Figure 26 and will be discussed.

To begin, panels from south and north orientations with the attachment of a “Type A” MFP on the exterior side are presented in Figure 26. In panel VS1A (Vancouver, south, position 1, “Type A” – Wood Fibre) the temperature variation between ambient exterior and interior surface of VS1A

achieved a maximum of 16.2°C in winter months while the average temperature difference for this period was 5.29°C. During fall, the measured differential temperature reached 13.9°C with an average of 4.5°C. For warmer ambient temperatures during the spring and summer months, “Type A” MFP demonstrated a strong performance with maximum records of 14.4°C and 14.7°C and averages of 5.6°C and 4.9°C for spring and summer months, respectively. Additionally, according to the temperature measurements for Panel VS4A (Vancouver, south, position 4, “Type A” – Wood Fibre) the south-east VS4A panel achieved an even better performance than VS1A throughout the data collection process. In the winter period, the difference between exterior and the interior surface temperature for panel VS4A achieved 19.13°C with an average of 5.57°C. For fall months the maximum measured temperature difference is 16.17°C with an average of 4.81°C. The spring period had the best average differential temperature for panel VS4A, 6.06°C, achieving a maximum of 16.37°C. For the summer months, 15.41°C of temperature variation was measured with an average of 5.18°C. As mentioned earlier, RSIs were calculated by applying the summation technique recommended by the ASTM-C1155/95-2013 standard. For panels VSA (Vancouver, south, “Type A”), the average calculated RSI was 3.78 m<sup>2</sup>\*K/W for the total assembly and 0.67 m<sup>2</sup>\*K/W for the MFP itself. The RSI was inversely proportional to the ambient outdoor temperature, continually lower in warmer months and higher in colder months.

Subsequently, for the north-positioned panels, the difference between interior and exterior temperature was smaller than their respective south-positioned panels. In winter months, the maximum difference achieved was 9.19°C with an average of 3.99°C for panel VN1A (Vancouver, north, position 1, “Type A” – Wood Fibre). Spring, summer, and fall months had similar maximum differences between exterior and interior temperatures, namely 8.81°C, 8.14°C, and 8.02°C respectively. The average performance was considerably different, as the spring period was

performing closer to the summer period by an average of 3.92°C, fall was slightly lower with an average of 3.15°C, and summer showed an average of 2.42°C. Panel VN4A (Vancouver, north, position 4, “Type A” – Wood Fibre) had similar thermal efficiency to VN1A. During the winter period, the maximum difference in temperature was 9.14°C with an average for the season of 4.06°C. The maximum differences in spring, summer, and fall were 8.45°C, 8.79°C, and 8.09°C, respectively. The average season performance, after winter, was better in spring with 3.75°C, followed by fall with 3.26°C, and summer with 2.34°C. The RSI calculations for Vancouver north positioned panels were not considered in this study due to technical issues with the heat flux sensors applied to these panels.

The results from panels with the “Type B” MFP are discussed below. The maximum variation between exterior and interior temperature of the VS2B (Vancouver, south, position 2, “Type B” – XPS), in the winter period, achieved up to 20.28°C during the peak hours of solar radiation and the average for the entire winter period was 5.47°C, as presented in Figure 26. The maximum variations for summer, spring, and fall are 17.13°C, 16.85°C, and 17.63°C, respectively. The average variation for each period was 5.74°C in spring, 4.69°C, in fall, and 4.98°C in summer. The VS5B (Vancouver, south, position 5, “Type B” – XPS) panel demonstrated similar performance to the VS2B panel as they are placed in the same orientation. The panel allows the heat from solar radiation to travel through the wall assembly and during winter months the variation between outside and inside temperature achieved a maximum of 21.97°C and an average for the period of 5.58°C. For spring, the maximum difference achieved was 18.31°C. The best average performance was achieved during the spring period, 6.17°C, followed by summer with 5.01°C and fall with 4.73°C. The maximum variation was higher in fall, 18.66°C, than spring, 18.31°C, and summer, 17.72°C. The average RSI calculated for VSB (Vancouver, south, “Type B”) panels was 2.37

$m^2 \cdot K/W$  and  $0.58 m^2 \cdot K/W$  for the MFP “Type B” in the Vancouver south-positioned panel itself. The impact of solar radiation can be seen by the variation in temperature of the panels. North-positioned panels always have lower temperature variation than south-positioned panels. VN2B (Vancouver, north, position 2, “Type B” – XPS) achieved the maximum variation in temperature of  $9.71^\circ C$  and average variation of  $4.26^\circ C$ , both in the winter period. The winter performance is followed by spring, fall, and summer with averages of  $3.96^\circ C$ ,  $3.31^\circ C$ , and  $2.219^\circ C$ . The maximum difference in temperature for VN2B increases from  $7.86^\circ C$  in the fall, to  $8.11^\circ C$  in the summer, and  $8.53^\circ C$  in the spring period.

The panel VN5B (Vancouver, north, position 5, “Type B” – XPS) has slightly better performance than panel VN2B, achieving  $10.14^\circ C$  as a maximum variation of temperature and averaging  $4.59^\circ C$  in the winter period. The maximum difference measured between exterior temperature and interior layer of the panel is followed by the spring period,  $8.90^\circ C$ , summer period,  $8.37^\circ C$ , and fall period,  $8.34^\circ C$ . The averages for spring, summer, and fall are  $4.17^\circ C$ ,  $2.34^\circ C$ , and  $3.56^\circ C$ , respectively.

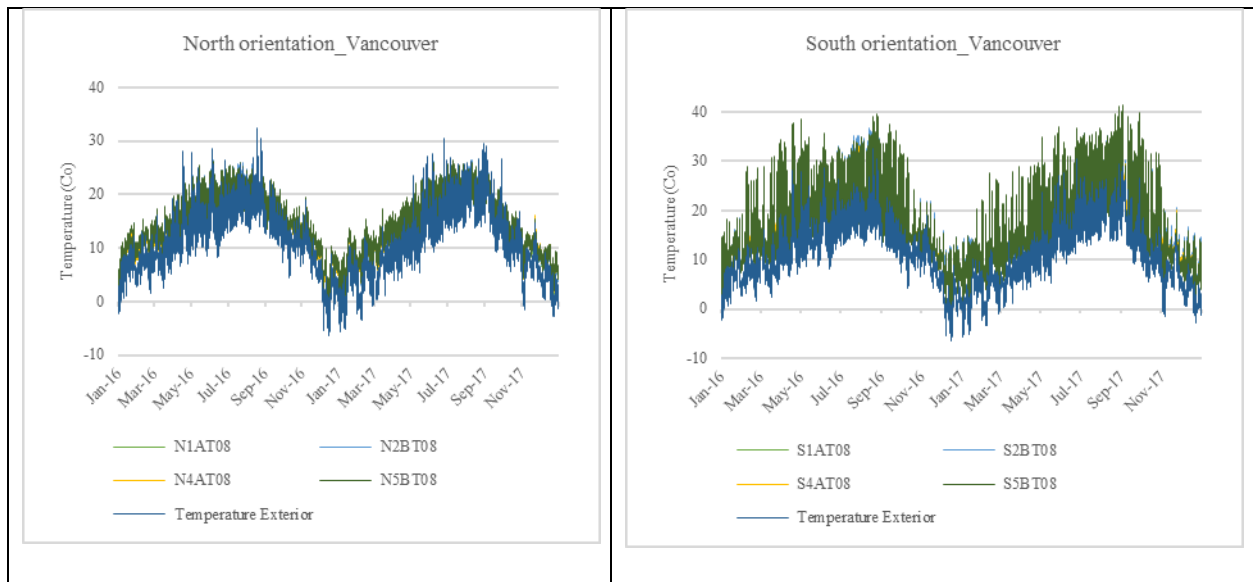


Figure 26: Temperature on the interior surface of MFPs and exterior temperature profiles based on 2 years of data for Vancouver north/south orientations.

Second, results from the Edmonton location are presented in Figure 27. The maximum variation between exterior temperature and the temperature in the interior layer of ES1A (Edmonton, south, position 1, “Type A” – Wood Fibre) measurement was 33.07°C and the average for the period was 10.41°C. Spring and fall demonstrated similar results with an average of 7.07°C and 7.22°C and maximum measurements of 26.01°C and 25.62°C. In the summer period the maximum difference between exterior and interior decreased to 16.35°C with an average of 5.75°C. As panel ES4A (Edmonton, south, position 4, “Type A” – Wood Fibre) faces south-east, the variation between indoor and outdoor temperature is slightly higher than south-west facing panel ES1A. The maximum variation of 33.12°C was achieved during the winter period and the average for the period was 11.01°C. As expected, results from ES1A and ES4A are similar and spring and summer periods show maximum variations in temperature of 25.61°C and 25.58°C with an average of 7.23°C and 7.49°C. Summer demonstrated a smaller variation of indoor and outdoor temperature of 16.68°C with an average of 5.79°C. The RSI calculated in ESA (Edmonton, south, “Type A”) was 3.09 m<sup>2</sup>\*K/W for the total wall assembly on average and 0.67 m<sup>2</sup>\*K/W for the MFP.

On the other hand, “Type A” panels positioned facing north demonstrated lower indoor and outdoor temperature differences than south-facing panels. For panel EN1A (Edmonton, north, position 1, “Type A” – Wood Fibre) the variation in the winter period achieved a maximum of 16.12°C with an average of 7.01°C as presented in Figure 27. The maximum measurements were found in spring (15.46°C), fall (13.12°C), and summer (10.58°C) with average values of 4.55°C, 4.90°C, and 3.31°C. The results from indoor and outdoor temperature variation from panel EN1A and EN4A are similar as they are both positioned facing north in Edmonton. The maximum difference measured for panel EN4A (Edmonton, north, position 4, “Type A” – Wood Fibre) was in the winter period and achieved 15.72°C with an average of 7.04°C for the period. The maximum

variations measured in spring, fall, and summer were 15.03°C, 13.39°C, and 10.09°C, with average measurements of 4.42°C, 4.82°C, and 3.16°C. The RSI calculated for ENA panels was 3.19 m<sup>2</sup>\*K/W on average for the total wall assembly and 0.72 m<sup>2</sup>\*K/W for the MFP.

The results for panels with MFP “Type B” are presented next. The maximum variation between outdoor and interior temperature for panel ES2B (Edmonton, south, position 2, “Type B” – XPS) was measured in the winter period and achieved as high as 35.57°C with an average for the period of 10.51°C. Fall and spring periods had similar measurements, achieving maximum differences of 27.65°C and 27.83°C and averaging 7.21°C and 6.96°C. During the summer months the maximum difference achieved was 17.86°C with an average for the period of 5.47°C. Similar results were found between panels ES2B and ES5B. The maximum difference in temperature for panel ES5B (Edmonton, south, position 5, “Type B” – XPS) was measured in winter months achieving 35.36°C with an average of 10.56°C. Measurements from fall and spring months were similar, with a maximum difference of 28.33°C and 28.39°C for fall and spring, respectively, and averages of 7.20°C and 7.05°C. In the summer period the maximum difference measured was 18.76°C with an average of 5.59°C. The RSI calculation for ESB (Edmonton, south, “Type B”) was not considered in this study for the final analyses due to some technical issues such as the malfunctioning of some of the sensors.

The analysis of panels ENB (Edmonton, north, “Type B”) are presented as follows. The measurements for EN2B (Edmonton, north, position 2, “Type B” – XPS) reveal a maximum variation of 17.15°C and the average for winter was 7.72°C. The maximum variations achieved were 16.24°C, 13.29°C, and 8.94°C in spring, fall, and summer. The averages measured for the period were 5.18°C, 4.47°C, and 2.82°C. The measurements for panel EN5B (Edmonton, north, position 5, “Type B” – XPS) are comparable with the results from panel EN2B. The maximum

difference in temperature, 16.18°C, occurred during the winter with an average of 7.47°C for the period. Maximum measurements of 16.31°C, 12.74°C, and 10.09°C were found in spring, fall, and summer, and the average variation for the period was 4.42°C, 4.82°C, and 3.16°C. The RSI calculated for the total wall assembly of ENB (Edmonton, north, “Type B”) panels was 2.87 m<sup>2</sup>\*K/W on average and 0.72 m<sup>2</sup>\*K/W for the MFP.

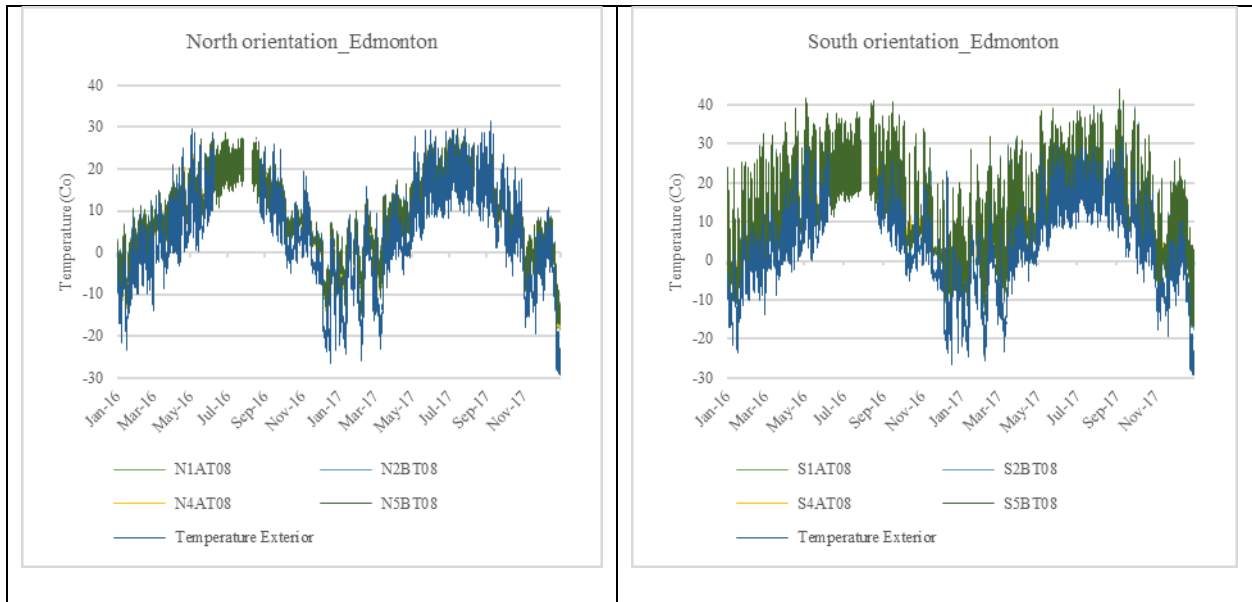


Figure 27: Temperature on the interior surface of MFPs and exterior temperature profiles based on 2 years of data for Edmonton north/south orientations.

Another important aspect of this study, it is the impact of the weather conditions on the material’s performance. In this regard, comparisons between results from “Type A”, “Type B” and “Type C” in both locations (Vancouver and Edmonton) were also made selecting the calculated RSI results from the months of January and June. As represented in Figure 28, the RSI calculated were lower at summer months than at winter months.

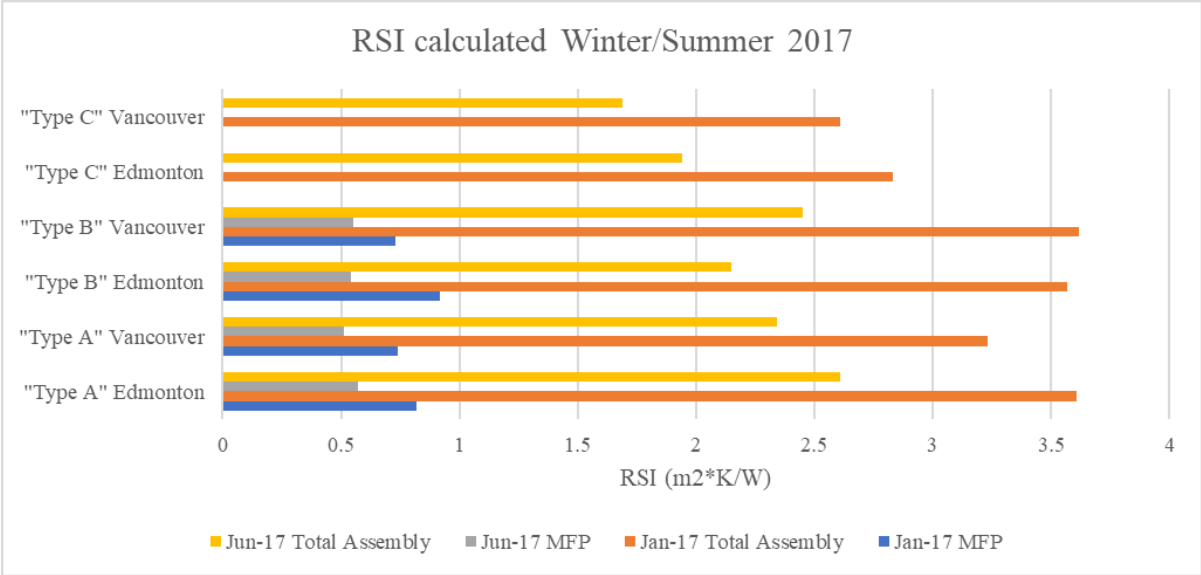


Figure 28: RSI calculated for all wall types in January and June, for both locations.

To achieve an overall evaluation of the hygrothermal performance of the MFPs, discussion of the MC, relative humidity, and climatic conditions are necessary. In this study, MC and temperature profiles were measured over a period of two years. The sensors were applied at three heights on the inner and outer layers of the wall assemblies in two locations. It was found that for panels tested in Vancouver, based on the vertical MC gradient for the exterior of the MFP in all three types of wall assemblies, the MC level at the upper location was slightly higher than at the bottom and middle, within 2%, for north-facing test panels. The differences among these three measurement points for the south-facing test panels were minimal. In the interior layer the difference in MC among these three measurements was less than 0.5%. For panels tested in Edmonton, no significant vertical temperature or MC profiles were observed for the interior or exterior layers measured. The temperature sensors in all cases were inversely proportional to the MC levels. In warmer months the MC levels for both MFPs were lower than in colder months for both locations (Edmonton and Vancouver). The maximum MC for both orientations, locations, and types of material were measured in January and the lowest MC was measured in July.

Both MFPs evaluated in this thesis were developed by FPInnovations, a Canadian non-profit organization that has been working on energy-efficient strategies for building envelope. FPInnovations provided a report with information about the product’s design, expected thermal efficiency, and MC simulated results. In the MFP report provided by FPInnovations (Knudson, Pirvu, Wang, & Symons, 2014) MC simulations were carried out for both climate zones (Edmonton and Vancouver). WUFI Software was used to obtain the simulated results and the parameters are described in Table 12.

Table 12: Parameters used for WUFI simulations for Moisture Content.

	Layer	Material	Layer thickness mm	Climate zone
1st	Exterior	Regular Lime Stucco	20	
2nd	Vantilated air layer	Treated Wood Strapping	20	
3rd	Building wrap	Tyvek type	0.2	
4th	Sheathing	1/4" OSB - Outside skin	6.4	Zone 5 - Vancouver and Zone 7 - Edmonton
5th	Rigid insulation	XPS	25	
6th	Sheathing	Wood Fibre	40	
7th	Cavity (5.5 in)	1/4" OSB - inside skin Glass fiber batt insulation	6.4	
8th	Vapor retarder	2x6 spruce	140	
8th	Vapor retarder	Vapor retarder, 5 perm	1	
9th	Interior	Interior Gypsum	12.5	

The simulated results were compared to the real data provided by the MC sensors affixed to the inner and outer layer of the MFPs as presented in Figure 29. For the inner and outer layers of the MFP “Type A”, the minimum MC levels were lower than the simulated results for both locations, but the maximum MC was lower in Vancouver than in Edmonton. The minimum MC in Vancouver and Edmonton for “Type B” were also lower than simulated results. For the inner layer, the maximum MC measurement for Vancouver was almost the same as the simulated results, but

in Edmonton the real measurements were lower than the simulated measurements. For the outer layer of “Type B”, the real data shows higher measurements than the simulated results as presented in Figure 29.

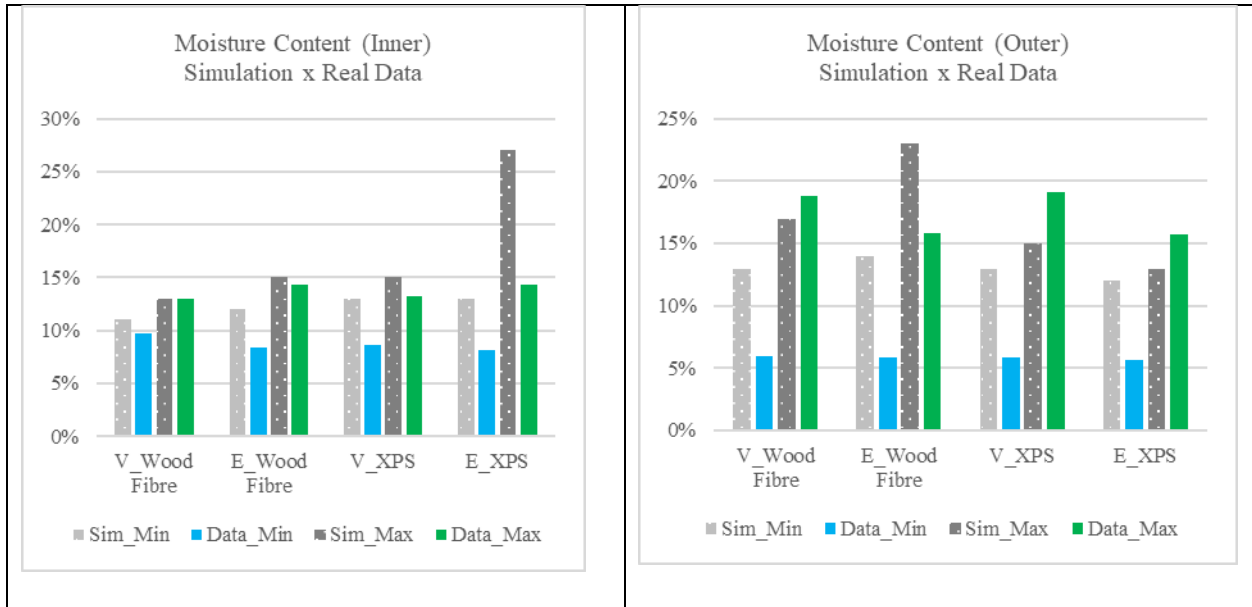


Figure 29: Moisture content comparison between simulated and field results.

## **Chapter 5 Conclusion**

In this chapter, a general conclusion from the hygrothermal performance evaluation of the MFPs will be presented, followed by the research contributions from this study. Then, some limitations of this research are summarized and finally, recommendations for future studies are proposed.

### **5.1 General Conclusion**

The focus of this research was to evaluate the hygrothermal performance of two innovative MFPs (which can be used for both new and existing buildings) in two different climatic conditions. In order to achieve this goal, two test huts were built with three types of wall assemblies at different orientations, and nearly 200 sensors (temperature, heat flux, humidity, moisture content) and a weather station were employed in each test hut. Measurements from these sensors were analyzed and various hygrothermal parameters such as thermal distribution, thermal bridging, wood thermal mass performance, thermal resistance, moisture content levels, humidity levels, and impact of the weather conditions were then investigated in this research project.

According to the vertical temperature distribution, discussed in Chapter 4, within each wall assembly, it is found that the attachment of either of the MFPs to the exterior side of the conventional wall assembly contributed to an improvement in the vertical temperature distribution for both types of wall assemblies in any orientation in both locations (Edmonton, Vancouver) when comparing with the “Type C” conventional wall assembly. Also, as discussed in Chapter 4, the horizontal temperature distribution demonstrated by the “Type A” wall assembly demonstrated a better performance of heat flow in its inner layers than “Type B” and “Type C” wall assemblies.

Furthermore, the RSI values were analyzed. It was found that when considering the overall performance of the wall assemblies, the “Type A” wall assembly, with a wood fibre panel attached to its exterior, has a higher thermal resistance than both the “Type B” assembly, with XPS attached

to its exterior, and the “Type C” assembly, with no panel attached, in both locations (Edmonton and Vancouver). The final RSI results are represented in Figure 30.

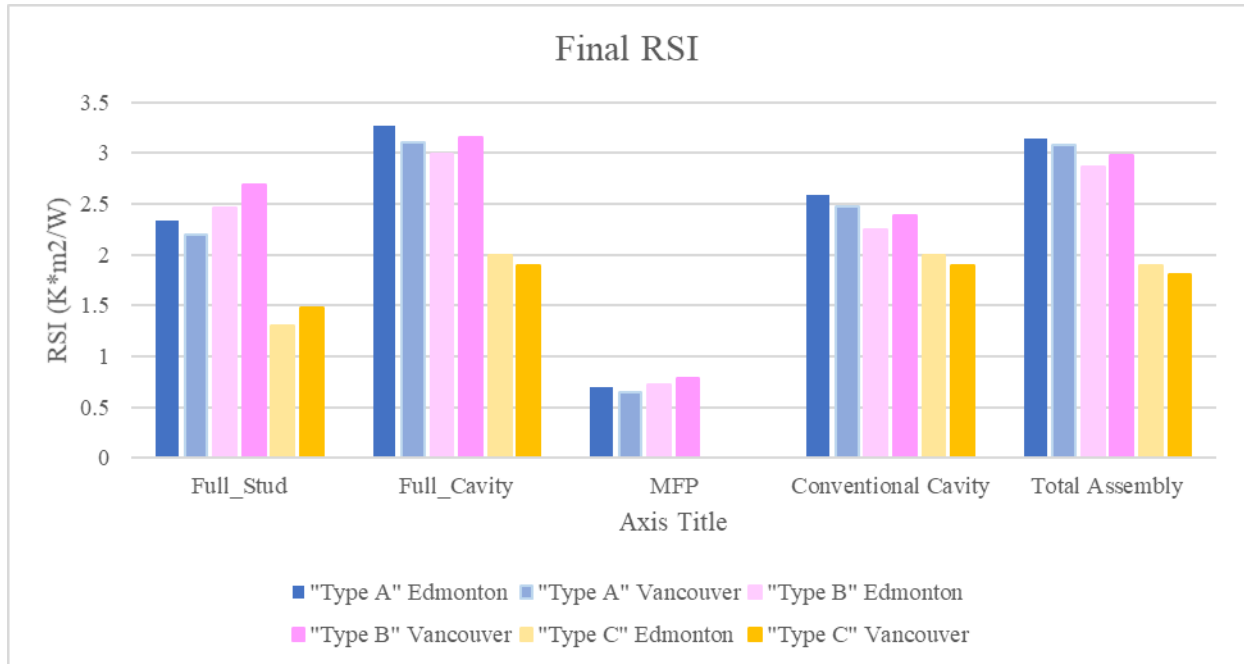


Figure 30: Results RSI, All wall assemblies, and locations.

It is important to note, however, that when considering only the RSI measured on the MFP, “Type B” performs better on average than “Type A”. It is thus concluded that other factors such as moisture content and climate conditions are also crucial when discussing the overall wall assembly performance. For this reason, when analyzing other factors involved in the hygrothermal performance, it was found that in a severe climatic condition like Edmonton, “Type A” performs better than “Type B” for both orientations. In a moderate climate like Vancouver, “Type B” performs better than “Type A” on north-oriented panels where the high moisture content levels and the lower levels of solar radiation are able to dry out the moisture trapped within the wall assembly layers. For south-positioned panels in Vancouver, “Type A” performs better than “Type B” on average.

Additionally, on south-facing walls in both locations, the variations in temperature throughout the layers of the wall assemblies were significantly higher than that of the north-facing walls due to the impact of solar radiation. In most cases, “Type A” and “Type B” assemblies demonstrated similar performances, but when considering “Type C” with no attachment of MFP as a baseline, it was concluded that the attachment of an MFP to the exterior side of the wall helped to regulate the interior temperature gradients and improve the overall thermal performance of the wall assemblies.

Another important aspect when analyzing hygrothermal performance of the building envelope is the moisture content levels. With the data collected from 176 moisture content sensors, it was found that on average moisture content levels for the “Type A” and “Type B” wall assemblies were higher in Vancouver than in Edmonton. Also, for the outer layer of the MFPs, the moisture content was higher than that of the inner layers, as presented in Figure 31. While with the “Type C” wall assembly, there is a noticeable improvement in lowering moisture content levels through the wall.

It was also found that there is a significant difference in terms of moisture content profiles between north and south orientations. Typically, there are higher moisture content levels in north-positioned walls by up to 8% and distinct seasonal variation; while for south-oriented walls, a greater daily fluctuation is observed, but it is less significant than seasonal variation, and the influence of orientation in Edmonton is much smaller than in Vancouver.

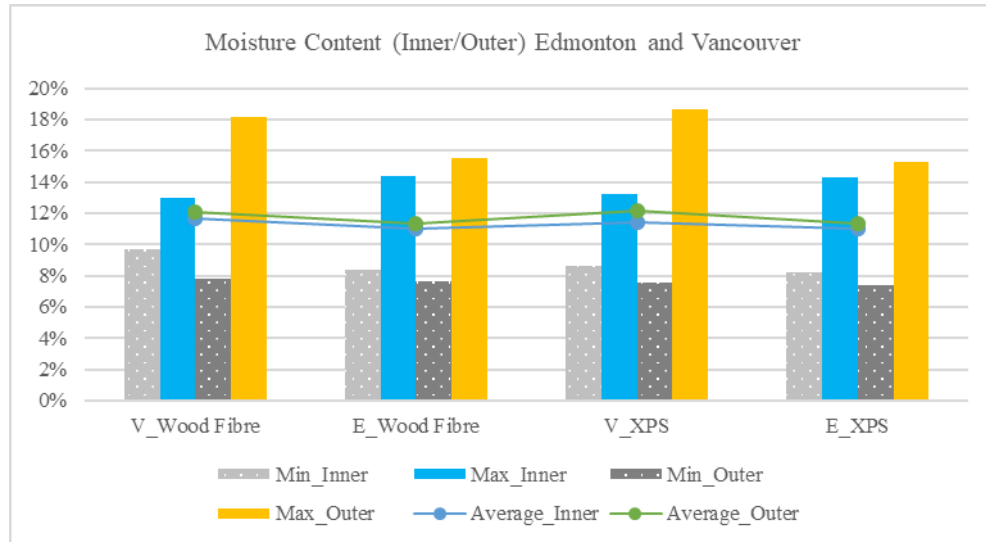


Figure 31: Moisture content levels for inner and outer layers of MFPs in Edmonton and Vancouver locations.

In conclusion, the attachment of either “Type A” or “Type B” MFPs significantly improved temperature distribution and moisture control of the wall assemblies. To be specific, the wood-fibre “Type A” MFP had a slightly better overall performance than the XPS “Type B” MFP in the severe climatic condition of Edmonton for both orientations. In the moderate climatic condition of Vancouver, for the north-oriented wall, “Type B” performed better than “Type A”; and for the south-oriented wall assembly, “Type A” performed better than “Type B”. However, when comparing with the “Type C” wall assembly, the addition of either of the MFPs significantly improved the overall hygrothermal performance of the building envelope of the test huts analysed in this research.

## 5.2 Research Contributions

The research presented in this thesis offers the following contributions:

- Field test analyses of the use of wood fibre—which is environmentally-friendly and 100% recyclable—in residential applications.

- The validation for introduction of a new environmentally-friendly technology to the Canadian homebuilding market and consequently to Canada's economy.
- Holistic understanding of hygrothermal performance of multi-functional panels attached to the exterior side of the building envelope under cold climate conditions.
- The gained knowledge of long-term experimental field analysis of multi-functional panels to test energy efficiency under different climatic conditions.

### **5.3 Research Limitations**

This research is subject to the following limitations:

- The testing was conducted under unoccupied conditions; the long-term testing was conducted in test huts built in Edmonton and Vancouver, Canada.
- Economic analyses were not included in this research, such as cost for materials, installation costs, and possible energy savings.
- The hygrothermal performance evaluation of the multi-functional panels did not include the connections with windows and doors, only wall assemblies.

### **5.4 Future Research**

Based on the research presented in this thesis, the recommendations for future work include:

- Testing in various climatic conditions is recommended mostly because neither of the climates included in this study present continually warm or cold temperatures throughout the year.
- Testing in actual houses under occupied conditions is also recommended for both types of multi-functional panels to evaluate the impact on moisture levels and overall hygrothermal performance.

- Applicability in real houses by testing connections with windows, door, and roof, and the impact of these connections on the overall performance evaluation of the multi-functional panels.
- Validation of the test results by conducting detailed hygrothermal performance simulations.

## References

- Aflaki, A., Mahyuddin, N., & Baharum, M. R. (2016). The influence of single-sided ventilation towards the indoor thermal performance of high-rise residential building: A field study. *Energy and Buildings*, *126*, 146–158. <https://doi.org/10.1016/j.enbuild.2016.05.017>
- Asdrubali, F., & Baldinelli, G. (2011). Thermal transmittance measurements with the hot box method: Calibration, experimental procedures, and uncertainty analyses of three different approaches. *Energy and Buildings*. <https://doi.org/10.1016/j.enbuild.2011.03.005>
- Asdrubali, F., D'Alessandro, F., Baldinelli, G., & Bianchi, F. (2014). Evaluating in situ thermal transmittance of green buildings masonries—A case study. *Case Studies in Construction Materials*, *1*, 53–59. <https://doi.org/10.1016/j.cscm.2014.04.004>
- ASHRAE. (1991). *1991 ASHRAE Thermal Mass Credits Related to Building Envelope*.
- ASTM. (2013). *ASTM C 1155: Standard Practice for Determining Thermal Resistance of Building Envelope Components from the In-Situ Data*. Retrieved from <https://civilengineersstandard.com/wp-content/uploads/2018/11/C-1155.pdf>
- Awad, H., Gül, M., Zaman, H., Yu, H., & Al-Hussein, M. (2014). Evaluation of the thermal and structural performance of potential energy efficient wall systems for mid-rise wood-frame buildings. *Energy and Buildings*, *82*, 416–427. <https://doi.org/10.1016/j.enbuild.2014.07.032>
- Azari, R., Garshasbi, S., Amini, P., Rashed-Ali, H., & Mohammadi, Y. (2016). Multi-objective optimization of building envelope design for life cycle environmental performance. *Energy and Buildings*, *126*, 524–534. <https://doi.org/10.1016/j.enbuild.2016.05.054>

- Beaundry, K., & MacDougall, C. (2019). Structural performance of non-plastered modular straw bale panels under transverse and gravity loads. *Construction and Building Materials*, 216, 424–439.
- Bienvenido-Huertas, D., Moyano, J., Marín, D., & Fresco-Contreras, R. (2019). Review of in situ methods for assessing the thermal transmittance of walls. *Renewable and Sustainable Energy Reviews*. <https://doi.org/10.1016/j.rser.2018.12.016>
- Biks, Y., Ratushnyak, G., & Ratushnyak, O. (2019). ENERGY PERFORMANCE ASSESSMENT OF ENVELOPES FROM ORGANIC MATERIALS. *Architecture, Civil Engineering, Environment*, 12(3), 55–67. <https://doi.org/10.21307/acee-2019-036>
- Binici, H., Eken, M., Dolaz, M., Aksogan, O., & Kara, M. (2014). An environmentally friendly thermal insulation material from sunflower stalk , textile waste and stubble fibres. *Construction and Building Materials*, 51, 24–33. <https://doi.org/10.1016/j.conbuildmat.2013.10.038>
- Boukhattem, L., Boumhaout, M., Hamdi, H., & Benhamou, B. (2017). Moisture content influence on the thermal conductivity of insulating building materials made from date palm fibers mesh. *Construction and Building Materials*, 148, 811–823. <https://doi.org/10.1016/j.conbuildmat.2017.05.020>
- Chen, W., Hao, H., Chen, S., & Hernandez, F. (2015). Performance of composite structural insulated panel with metal skin subjected to blast loading. *JMADE*, 84, 194–203. <https://doi.org/10.1016/j.matdes.2015.06.081>
- Cruz, C. O., Silva, C. M., Dias, P. V., & Teotónio, I. (2017). Economic impact of changing thermal regulation—An application to the city of Lisbon. *Energy and Buildings*, 149, 354–

367. <https://doi.org/10.1016/J.ENBUILD.2017.05.030>

Djamila, H., Rajin, M., & Rizalman, A. N. (2018). Energy efficiency through building envelope in Malaysia and Singapore. *Journal of Advanced Research in Fluid Mechanics and Thermal Sciences*, 46(1).

Edgars, L., Kaspars, Z., & Kaspars, K. (2017). Structural performance of wood based sandwich panels in four point bending. *Procedia Engineering*, 172, 628–633.

<https://doi.org/10.1016/j.proeng.2017.02.073>

ENERGY STAR Program-Canada. (2018). ENERGY STAR Multifamily High-Rise Pilot Program. Retrieved August 16, 2019, from <https://www.nrcan.gc.ca/buildings/energy-starr-multifamily-high-rise-pilot-program/21966>

Flanders, S. N. (1985). *The Convergence Criterion in Measuring Building R .. Values*. Atlanta: American Society of Heating, Refrigerating and Air-Conditioning Engineers.

Ge, H., & Baba, F. (2015). Dynamic effect of thermal bridges on the energy performance of a low-rise residential building. *Energy & Buildings*, 105, 106–118.

Ge, H., Wang, R., & Baril, D. (2017). Field monitoring of Hygrothermal performance of attic venting systems in extreme cold climate. In *15th Canadian Conference on Building Science and Technology*.

Gounni, A., Mabrouk, M. T., El Wazna, M., & Kheiri, A. (2019). Thermal and economic evaluation of new insulation materials for building envelope based on textile waste. *Applied Thermal Engineering*, 149, 475–483. <https://doi.org/10.1016/j.applthermaleng.2018.12.057>

Hagerstedt, S., & Arfvidsson, J. (2010). Comparison of field measurements and calculations of

- relative humidity and temperature in wood framed walls. In *15th International Meeting of Thermophysical Society* (pp. 93–101). Valtice, Czech Republic.
- Hernández-pérez, I., Xamán, J., Macías-melo, E. V., & Aguilar-castro, K. M. (2018). Experimental thermal evaluation of building roofs with conventional and reflective coatings. *Energy & Buildings*, *158*, 569–579. <https://doi.org/10.1016/j.enbuild.2017.09.085>
- IEA. (2017). IEA, Transition to Sustainable Buildings: Strategies and Opportunities to 2050, Executive Summary. Retrieved January 15, 2018, from <http://www.iea.org/Textbase/npsum/building2013SUM.pdf>
- Jang, H., & Kang, J. (2016). A stochastic model of integrating occupant behaviour into energy simulation with respect to actual energy consumption in high-rise apartment buildings. *Energy and Buildings*, *121*, 205–216. <https://doi.org/10.1016/j.enbuild.2016.03.037>
- Kawasaki, T., & Kawai, S. (2006). Thermal insulation properties of wood-based sandwich panel for use as structural insulated walls and floors. *Journal of Wood Science*. <https://doi.org/10.1007/s10086-005-0720-0>
- Kayello, A., Ge, H., Athienitis, A., & Rao, J. (2017). Experimental study of thermal and airtightness performance of structural insulated panel joints in cold climates. *Building and Environment*, *115*, 345–357. <https://doi.org/10.1016/j.buildenv.2017.01.031>
- Knudson, R. M., Pirvu, C., Wang, B. J., & Symons, P. D. (2014). *Development of Multi-Functional Wood Composite Panel Products for Next Generation Building Systems*. Retrieved from FPIinnovations.ca
- Korjenic, A., & Petránek, V. (2011). Development and performance evaluation of natural

- thermal-insulation materials composed of renewable resources. *Energy & Buildings*, 43, 2518–2523. <https://doi.org/10.1016/j.enbuild.2011.06.012>
- Kosny, J., Fontanini, A. D., Shukla, N., & Fallahi, A. (2018). Thermal performance analysis of residential attics containing high performance aerogel-based radiant barriers. *Energy and Buildings*, 158. <https://doi.org/10.1016/j.enbuild.2017.10.081>
- Lawania, K. K., & Biswas, W. K. (2016). Achieving environmentally friendly building envelope for Western Australia's housing sector: A life cycle assessment approach. *International Journal of Sustainable Built Environment*, 5(2). <https://doi.org/10.1016/j.ijbsbe.2016.04.005>
- Li, Y., Yu, H., Sharmin, T., Awad, H., & Gül, M. (2016a). A performance comparison of multi-objective optimization algorithms for solving nearly-zero-energy-building design problems. *Energy and Buildings*, 121(7), 11–21. <https://doi.org/10.1016/j.enbuild.2016.03.054>
- Li, Y., Yu, H., Sharmin, T., Awad, H., & Gül, M. (2016b). Towards energy-Efficient homes: Evaluating the hygrothermal performance of different wall assemblies through long-term field monitoring. *Energy and Buildings*, 121, 43–56. <https://doi.org/10.1016/j.enbuild.2016.03.050>
- Lstiburek, J. (2002). Moisture control for buildings. *ASHRAE Journal*, 36–41.
- Manyumbu, E., Martin, V., & Fransson, T. H. (2016). Modeling the long-term effect of climate change on building heat demand: Case study on a district level. *Energy and Buildings*, 126(8), 485–497. <https://doi.org/10.1016/j.enbuild.2016.05.036>
- Medina, M. A., King, J. B., & Zhang, M. (2008). On the heat transfer rate reduction of structural insulated panels (SIPs) outfitted with phase change materials (PCMs). *Energy*, 33(4), 667–

678. <https://doi.org/10.1016/j.energy.2007.11.003>

Mousa, M. A., & Uddin, N. (2012). Structural behavior and modeling of full-scale composite structural insulated wall panels. *Engineering Structures*, *41*, 320–334.

<https://doi.org/10.1016/j.engstruct.2012.03.028>

Mu, khopadhyaya, P., Ping, F., Kumaran, M., & Van Reenen, D. (2009). Role of vapor barrier in wood-frame stucco wall in variuos North American climates. *Journal of ASTM International*, *6*.

Mundt Petersen, S., & Harderup, L. (2015). Predicting hygrothermal performace in cold roofs using a 1D transient heat and mositure calculation tool. *Building and Environment*, *90*, 215–231.

Nik, V. M., Mata, E., Sasic Kalagasidis, A., & Scartezzini, J. L. (2016). Effective and robust energy retrofitting measures for future climatic conditions - Reduced heating demand of Swedish households. *Energy and Buildings*, *121*, 176–187.

<https://doi.org/10.1016/j.enbuild.2016.03.044>

NRCan-EcoEnergy. (2014). EcoENERGY for Renewable Power/Natural Resources Canada.

Retrieved January 28, 2018, from <https://www.nrcan.gc.ca/eoaction/14145>

NRCan-LEEP. (2019). LEEP-Local Energy Efficiency Partnerships/Natural Resources Canada.

Retrieved August 18, 2019, from <https://www.nrcan.gc.ca/energy-efficiency/energy-efficiency-homes/local-energy-efficiency-partnerships-leep/17338>

NRCan-NECB/C. (2017). National Energy Code of Canada for Buildings/Natural Resources

Canada. Retrieved August 18, 2019, from <https://www.nrcan.gc.ca/buildings/canadas->

national-energy-code/20675

- NRCan-Office of Energy Efficiency. (2016). Natural Resources Canada. Retrieved from <http://oee.nrcan.gc.ca/corporate/statistics/neud/dpa/showTable.cfm?type=AN&sector=res&juris=00&rn=11&page=0>
- Panjehpour, M., Ali, A., & Lei, Y. (2013). Structural Insulated Panels: Past, Present, and Future. *Journal of Engineering, Project, and Production Management*, 3, 2–8.
- Panyakaew, S., & Fotios, S. (2011). New thermal insulation boards made from coconut husk and bagasse. *Energy & Buildings*, 43(7), 1732–1739.  
<https://doi.org/10.1016/j.enbuild.2011.03.015>
- Radon, J., Pisello, A. L., Castaldo, V. L., & Piselli, C. (2016). On-site assessment of the discharge coefficient of open windows. *Energy and Buildings*, 126(8), 485–497.  
<https://doi.org/10.1016/j.enbuild.2016.05.026>
- Salonvaara, M., Karagiozis, A., Holm, A., et al. (2001). Stochastic building envelope modeling: The influence of material properties. *Integration of Building Envelopes, Performanc.*
- Sassine, E. (2016). A practical method for in-situ thermal characterization of walls. *Case Studies in Thermal Engineering*, 8, 84–93. <https://doi.org/10.1016/J.CSITE.2016.03.006>
- Semprini, G., Marinosci, C., Ferrante, A., & Predari, G. (2016). Energy management in public institutional and educational buildings: The case of the school of engineering and architecture in Bologna. *Energy and Buildings*, 126(2016), 365–374.  
<https://doi.org/10.1016/j.enbuild.2016.05.009>
- Simko, M., Krajč, M., Simko, P., & Kalús, D. (2018). Insulation panels for active control of heat

- transfer in walls operated as space heating or as a thermal barrier : Numerical simulations and experiments, *158*, 135–146. <https://doi.org/10.1016/j.enbuild.2017.10.019>
- Stergaard, D. S., & Svendsen, S. (2016). Case study of low-temperature heating in an existing single-family house - A test of methods for simulation of heating system temperatures. *Energy and Buildings*, *126*, 535–544. <https://doi.org/10.1016/j.enbuild.2016.05.042>
- Tariku, F., Kumaran, K., & Fazio, P. (2015). Application of a Hygrothermal model in energy , durability , and indoor humidity retrofit design. *Journal of Building Physics*, *39*(1), 3–34. <https://doi.org/10.1177/1744259114522400>
- UNEP. (2007). UNEP, Buildings and Climate Change: Status Challenges and Opportunities (2007). Retrieved from <https://www.unep.org/sbci/pdfs/BuildingandClimateChange.pdf>
- Vera, I., & Langlois, L. (2007). Energy indicators for sustainable development. *Energy*, *32*(6), 875–882. <https://doi.org/10.1016/j.energy.2006.08.006>
- Verbeke, S., & Audenaert, A. (2018). Thermal inertia in buildings: A review of impacts across climate and building use. *Renewable and Sustainable Energy Reviews*, *82*, 2300–2318. <https://doi.org/10.1016/j.rser.2017.08.083>
- Wang, Bras, R., Sivandran, G., & Knox, R. (2010). A simple method for the estimation of thermal inertia. *Geophysical Research Letters*. <https://doi.org/10.1029/2009GL041851>
- Wang, Q., Ploskić, A., Song, X., & Holmberg, S. (2016). Ventilation heat recovery jointed low-temperature heating in retrofitting - An investigation of energy conservation, environmental impacts and indoor air quality in Swedish multifamily houses. *Energy and Buildings*, *121*, 250–264. <https://doi.org/10.1016/j.enbuild.2016.02.050>

- Winkler, M., Nore, K., & Antretter, F. (2014). Impact of the moisture buffering effect of wooden materials on energy demand and confort conditions. In *10th Nordic Symposium on Building Physics* (pp. 483–491). Arfvidsson, Jesper.
- Zhou, Xiao-yan, Zheng, F., Li, H., & Lu, C. (2010). An environment-friendly thermal insulation material from cotton stalk fibers. *Energy & Buildings*, *42*(7), 1070–1074.  
<https://doi.org/10.1016/j.enbuild.2010.01.020>
- Zhou, Xiaohai, Derome, D., & Carmeliet, J. (2016). Robust moisture reference year methodology for hygrothermal simulations. *Building and Environment*, *110*, 23–35.  
<https://doi.org/10.1016/j.buildenv.2016.09.021>
- Žigart, M., Kovačič Lukman, R., & Premrov, M. (2018). Environmental impact assessment of building envelope components for low-rise buildings. *Energy*, *163*.  
<https://doi.org/10.1016/j.energy.2018.08.149>